5-16-2008

Interaction Effects in Nickel Nanowires Arrays

Ovidiu Cezar Trusca
University of New Orleans

Interaction Effects in Nickel Nanowires Arrays

A Thesis

Submitted to the Graduate Faculty of the
University of New Orleans
In Partial fulfillment of the
Requirements for the degree of

Master of Science
in
Physics

By

Ovidiu Cezar Trusca

BS in Metallurgical Engineering, Technical University Cluj-Napoca, Romania, 1989
MBA "Babes-Bolyai" University, Cluj-Napoca, Romania, 1999

May, 2008

Acknowledgments

I would like to thank first to Dr. Leonard Spinu, my advisor, who guided me throughout my whole experience as a graduate student. He gave me a lot of suggestions and his advice was always very valuable for me.

I would like to thank my Thesis Committee Members for their insightful suggestions, their help and guidance for this work: Dr. Leonard Spinu, my Committee Chair, Dr. John B. Wiley from the Department of Chemistry and Advanced Materials Research Institute (AMRI) (University of New Orleans) for providing the materials used in this work and for his continuous support and useful discussions, Dr. Leszek Malkinski from Department of Physics and AMRI (UNO) and Dr. Ashok Puri from the Department of Physics, who were always available when I needed their help.

I am deeply grateful to my colleagues Dr. Dorin Cimpoesu, Ms. Jin Hee Lim, Dr. Xiequn Zhang, Cosmin Radu, Dr Ioan Dumitru and Huy Pham for their support and valuable opinions. My work wouldn't have been possible without their continuous help and commitment.

I would like to thank all of my friends and colleagues from Department of Physics and AMRI (UNO) for their assistance. Also, I would like to thank Department of Physics and AMRI for making possible my teaching and research assistantships during these years.

I would like to thank Mrs. Sandra Merz, Mrs. Jennifer Tickle and Mr. Poncho De Leon for taking care of my paperwork during my study at UNO.

Also, I would like to thank to all the great professors I have met here, at UNO, who made all the difference in my life: Dr. G. Seab, Dr. J. Murphy, Dr. J. Ioup, Dr. G. Ioup, Dr. K. Stokes, Dr. M. Slaughter and Dr. J. Tang.

Finally, I would like to thank and dedicate this thesis to my family: my wife Maria, my mother Lina, my father Vasile, my brother Horatiu, and my sister-in-law Mariana, for their financial support and emotional contributions.

Table of Contents

List of Figures

List of Tables

Abstract

Systems of magnetic nanowires are considered strong candidates in many technological applications as microwave filters, sensors or devices for data storage. Because of their strong potential as candidates in such applications they became lately the object of many studies. However, due to the very complicated nature of the interwire interactions, their magnetic behavior is very difficult to be interpreted. The main parameter controlling the response of magnetic nanowires assemblies is the aspect ratio of the nanowires that is defined as the ratio of the length to the wire's diameter. In our study we choose to modify the aspect ratio by keeping a constant length of nanowires and modifying the wire's diameter while keeping the same interwire distance. The samples were studied at room temperature, using vibrating sample magnetometer and X-band ferromagnetic resonance experiments. The results are explained taking into account the effects of the magnetostatic interactions and shape anisotropy.

Key words: magnetic nanowires, magnetic interactions, hysteresis loop, ferromagnetic resonance, magnetic moment

Introduction

Nanostructured magnetic materials are the focus of many research efforts in the past few years, being very interesting not only from theoretical point of view, but also due to the wealth of their potential technological applications. Since 1991 the increase in storage density for commercially available hard disks has been 65% per year. Several companies reached the performance to have densities up to 130 Gbit/inch^2.[1] One approach to extend this limit is via perpendicular media, or using nanomagnets.[2] The density of recording media depends on the size of magnetic particles, the distance and the interaction among them, and using nanowires arrays, the problem of miniaturization can be solved.[3] Magnetic nanoparticles can also be used in biology to probe the micromechanics of cells and the torsion of DNA molecules. Such particles are also being explored in gene therapy. [4]

In contrast to spherical nanoparticles, nanowires exhibit degrees of freedom associated with inherent shape anisotropy. Ferromagnetic nanowires exhibit unique and tunable magnetic properties that are very different from those of bulk ferromagnetic materials, thin films and spherical particles. However, the characterization and understanding of the magnetic properties of nanowires arrays is still a challenging task, the complexity of the interactions among wires making difficult to interpret even the experimental results of classical characterization methods, like ferromagnetic resonance (FMR).[1-6] This motivates the strong interest in understanding the interaction in structures of parallel nanowires.[6-10]

The magnetic anisotropy of such arrays is determined mainly by two contributions: the shape anisotropy, with a magnetic easy axis parallel to the wire axis, and the magnetostatic coupling among wires, which can develop a magnetic easy axis perpendicular to the wire axis.[7,8] The magnetocrystalline anisotropy energy is usually much smaller than the shape anisotropy for

such systems in the case of magnetic material as nickel (Ni) and iron. For magnetic nanowires of cobalt the magnetocrystalline anisotropy can be significant.

The main parameter that controls the frequency response of magnetic nanowires assemblies is the aspect ratio of the nanowires, i.e., the length to diameter ratio. The aspect ratio can be tuned, for example, by changing the length of nanowires and keeping the same diameter of wires. In the case of template method for nanowires preparation this can be easily done using different electrodeposition times.

Preliminary studies were done in our group[8,9] on Ni electrodeposited nanowire samples with a constant diameter and different length of wires. The angular dependence of the FMR resonance field was investigated for each sample, and the results were explained using a total demagnetizing factor, that takes into account the effect of interwire interaction.

In the present work we chose to modify the aspect ratio of nanowires by keeping constant their length and modifying the nanowire's diameter. This approach is more challenging as it requires designing templates of different diameters but with the same average distance between channels. Moreover, during the electrodeposition the constant length of nanowires for different samples of different diameters is controlled more difficult. Series of samples of different diameters, with the same length and average distances between the centers of wires, are ideal candidates for verifying the models recently proposed[6] to describe the interactions in such systems. Two sets of Ni nanowires with diameters (d) of 40, 60, 80 nm, respectively, and a constant lengths (l) of 1000 nm and 500 nm were grown using standard electrodeposition technique in alumina templates. The interpore distance is D = 100 nm, measured center to center. By changing the nanowires diameter, the aspect ratio m changes, and in this way the magnetic properties of these arrays, as the coercivity, saturation field, saturation magnetization and the

value of the resonance field for the same orientation of the samples, change. Moreover, the angular dependence of the resonance field was observed to have the shape consistent with presence of magnetostatic interactions in the nanowire arrays[8,9]. The samples with the same interpore distances and different diameters of wires show an increase in the peak of the angular dependence of the resonance field with the decrease in the aspect ratio. This behavior can be explained by the fact that increasing the diameter of the wires, the distance between two neighboring wires decreases and the interaction among them becomes larger.

The present work is organized as follows:

Chapter 1. *Overview of Magnetism.* This chapter gives an overview of the background information required for a full understanding of the remainder of the thesis. The background information includes the overview of the magnetic free energy including magnetocrystalline anisotropy, shape anisotropy and ferromagnetic resonance.

Chapter 2. *Experiment*. This chapter begins with a brief description of the method used to obtain the Anodized Aluminum Oxide (AAO) templates and a description of the method used to grow the nanowires into the AAO template by electrodeposition. The magnetostatic experiments using the Vibrating Sample Magnetometer are also presented in this chapter. The last part of the chapter is dedicated to the ferromagnetic resonance (FMR) experiments performed at room temperature using a X-band Bruker spectrometer.

Chapter 3. *Results and Discussions*. In this chapter the results of the measurements performed with the VSM and FMR are presented and explained.

Chapter 4. *Modeling of Interactions in Ferromagnetic Nanowires*. In this chapter a theoretical approach is used to explain the angular dependence of the resonance field for the nanowire samples.

Chapter 5. *Conclusions and Future Work.* This chapter gives out the conclusions of all work done in this thesis followed by prospects regarding more complicated structures such as nanotubes and core-shell structures.

Chapter 1: Overview of Magnetism

1.1 Magnetic Hysteresis Loop of Nanowires

The behavior of nanostructured magnetic materials can be characterized using magnetization hysteresis loops. The hysteresis loop is the magnetic response of a magnetic sample subjected to an external field. In our experiments the external magnetic field is applied parallel to the nanowire axis or perpendicular to it. The hysteresis loop obtained in such a manner has features dependant on the material, the size, the shape of the sample, and the orientation of the applied magnetic field with respect to the sample. Moreover, for arrays of nanoparticles the hysteresis loop depends also on the interactions between the individual particles. A typical magnetization hysteresis loop for a nanowires array is presented in Figure 1.1.

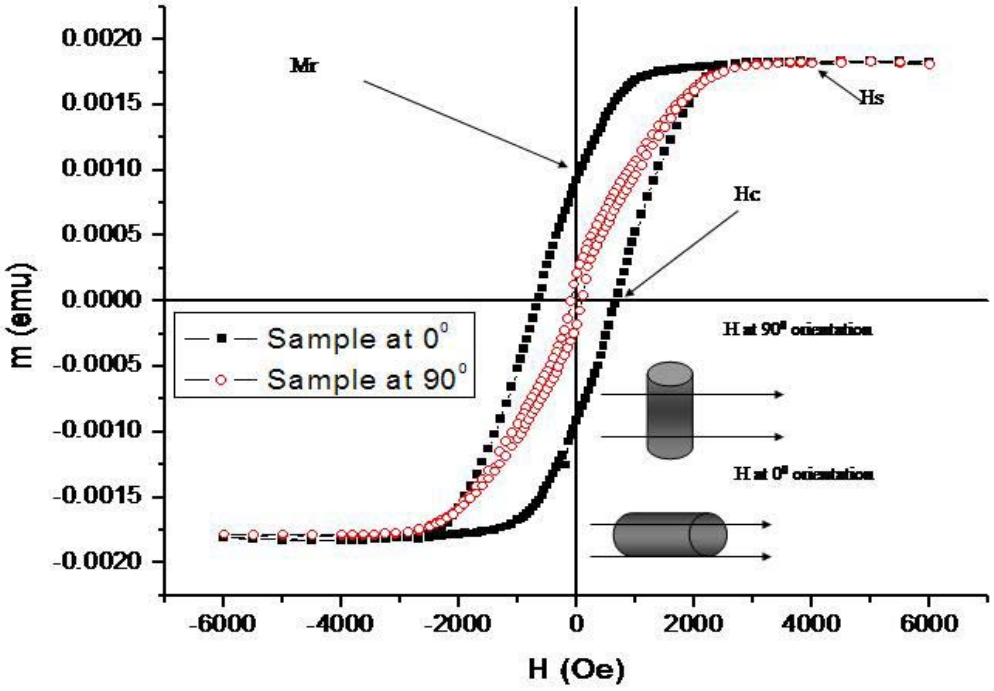

Figure 1.1 Magnetic hysteresis loop for a nanowire array with wire diameter of 80 nm and length of 1000 nm.

The hysteresis loop is described by several parameters:

a) The saturation magnetization, M_s

b) The remanent magnetization, M_r

c) The coercivity, H_c

d) The saturation field, H_s

The applied magnetic field at which the magnetization M becomes zero is called the coercive field or coercivity H_c. The saturation field H_s is the field needed to reach the saturation magnetization. The remanent magnetization M_r is the magnetization at $H = \boldsymbol{0}$. For nanostructures, such as an array of nanowires, the coercivity H_c, the saturation magnetizationM_s, and the remanent magnetization M_r are strongly dependent on the orientation of the applied magnetic field, and also on the size and shape of the sample.

The saturation magnetization M_s is obtained when all magnetic moments in the material are aligned in the same direction. Saturation magnetization M_s is a property of ferromagnetic materials, therefore it does not depend of the nanowire geometry. For an arbitrary nanowires array all of these characteristic magnetic properties can be tuned by choosing appropriately the material of the nanowires and also the nanowires dimensions. The magnetic behavior of a magnetic system can be explained starting from the magnetic free energy Thus, static properties, as the magnetization hysteresis loop, and dynamic properties, as the ferromagnetic resonance, can be explained by minimizing the total free energy of the magnetic system and this process is explained in the following.

1.2 Magnetic Free Energy

In this section we are interested in the energy of a magnetic system. We know that the problem of investigating the static equilibrium of a system is related to minimizing the total free energy of the system. In the Stoner–Wohlfarth model, by finding the total energy minima, it is possible to predict the magnetization rotation and switching behavior of a particle under the influence of an applied field.[11] Another example is that the existence of well-known domain structure in ferromagnetic materials can be explained by the result of minimization of the total free energy. Generally speaking, in observing the magnetic behavior of a magnetic system, it is important to understand what and how energy terms are playing a role in contribution of the total free energy of the whole system.

1.2.1 Magnetocrystalline anisotropy

The disposition of the magnetic moments in a magnetic crystal reflects the symmetry of the lattice. The symmetry of the crystal influences the interactions of the magnetic moments among themselves and with the lattice as well, and gives rise to anisotropic energy contributions. The sum of all these contributions is known as magnetocrystalline anisotropy.[12] Due to the magnetocrystalline anisotropy, there are directions in the space lattice in which is easier to magnetize a given crystal, and these directions are called easy directions. For a simplified case of uniaxial magnetic anisotropy, we suppose the uniaxial anisotropy axis, or the easy axis, is parallel to the c-axis of the crystal. In this case, we can say that the anisotropy energy is invariant with respect to rotations around the anisotropy axis, depending only on the relative orientation of magnetization vector **M** with respect to the axis. As **M** rotates away from the c-axis, the

anisotropy energy initially increases with θ, the angle between the c-axis and the magnetization vector, then reaches a maximum value at $\theta = 90^0$ and decreases to its original value at $\theta = 180^0$. So, the minimum anisotropy energy is obtained when the magnetization points either in the negative or positive direction along the c-axis. The energy density in this case can be expressed as:

$$W_K = K_0 + K_1 \sin^2\theta + K_2 \sin^4\theta + ..., \qquad (1.1)$$

the coefficients K_n, where $n = 0, 1, 2\ldots$, are called anisotropy constants, having dimensions of energy per unit volume. The higher-order terms above K_2 can be neglected because they are in general very small. The first term, K_0 is a constant, so it can be disregarded as well. Therefore, for small deviations of the magnetization vector from the equilibrium position, the anisotropy density can be approximated using the second term of equation 1.1 as:

$$W_K \cong K_1\theta^2 \cong 2K_1 - 2K_1\cos\theta = 2K_1 - \mathbf{M}\cdot\mathbf{H}_K \qquad (1.2)$$

In equation 1.2, $H_K = 2K_1/M_s$, symbolizes the anisotropy field, and it gives a measure of the strength of the anisotropy effect and of the torque necessary to take the magnetization away from the easy axis. M_s is the magnitude of the magnetization vector **M**. An example of magnetic material with uniaxial magnetocrystalline anisotropy is cobalt. The values of the first two anisotropy constants for cobalt at room temperature are $K_1 = 45\text{x}10^5$ erg/cm^3 and $K_2 = 15\text{x}10^5$ erg/cm^3.[11]

In the case of cubic crystals, the anisotropy energy can be expressed in terms of the direction cosines ($\alpha_1, \alpha_2, \alpha_3$) of the magnetization vector with respect to the three cube edges:

$$W_K = K_1\left(\alpha_1^2\alpha_2^2 + \alpha_2^2\alpha_3^2 + \alpha_3^2\alpha_1^2\right) + K_2\alpha_1^2\alpha_2^2\alpha_3^2 \qquad (1.3)$$

Both Fe and Ni have a cubic magnetocrystalline anisotropy but Fe has the easy axis along <100> direction while Ni along <111>.[11]

1.2.2 Magnetostriction and stress anisotropy

During the magnetization process the shape and the volume of a magnetic specimen change. This phenomenon is called magnetostriction and is due to the fact that the crystal lattice inside each domain is spontaneously deformed in the direction of domain magnetization, therefore generating the deformation of the entire specimen. For isotropic magnetostriction, the magnetoelastic energy density is given by:

$$W_\sigma = \frac{3}{2}\lambda_s \sigma \sin^2 \theta_s, \qquad (1.4)$$

where θ_s is the angle between the magnetization and the stress direction, λ_s is the appropriate magnetostriction constant, and σ is a uniaxial stress applied along a certain direction. For example, in the case of Ni the magnetostriction coefficient is -24.3 x 10^{-6} ergs/cm^3.[12]

1.2.3. Shape anisotropy

The magnetization is independent of the orientation of the applied field for a spherical object, but for a non-spherical object it is easier to magnetize it along its long axis than along its short axis. Therefore, if we consider a magnetized rod-shaped object, with a north pole at one end and the south at the other, the field lines will emerge from the north pole to the south pole. Inside the material the field lines are oriented from the south pole to the north pole, and are opposed to the magnetization of the material, since the magnetic moment points from the south pole to the north pole. The result is that the magnetic field inside the material tends to demagnetize the material. This field is called demagnetizing field $\mathbf{H_d}$ and acts in the opposite direction from the magnetization **M** which gives rise to it. Between the demagnetizing field and the magnetization there is a proportionality relation:

$$\mathbf{H}_d = -N_d \mathbf{M} \qquad (1.5)$$

Where N_d is the demagnetizing factor and it depends on the shape of the object. The demagnetizing factor can only be calculated exactly for an ellipsoid where the magnetization is uniform throughout the sample.[4]

The magnetostatic energy W_D, depends on the specific direction of the magnetization vector and it can be written as:

$$W_D = \frac{1}{2}\left(N_a M_x^2 + N_b M_y^2 + N_c M_z^2\right), \qquad (1.6)$$ where

N_a, N_b, N_c are the demagnetization factors pertaining to the three principal axes. Energy has the same mathematical form as the first-order uniaxial anisotropy, even though their physicals origins are different. So, in this case the magnetostatic self-energy is called shape anisotropy.

In general, for an ellipsoidal object, with the ellipsoid semi-axes a, b, and c, the demagnetization factors along the ellipsoid's semi-axes are: N_a, N_b and N_c, respectively. The relation that connects them is:

$$N_a + N_b + N_c = 4\pi \qquad (1.7)$$

In Figure 1.2 are presented three ellipsoids that can be used as theoretical representations of a nanowire: the prolate spheroid (ellipsoid of revolution), where $c > a = b$; the slender ellipsoid where $c >> a > b$, and the oblate spheroid where $c = b > a$.

a. Prolate spheroid

The prolate ellipsoid (Figure 1.2.a) is for interest as an approximation for a single-component nanowire with circular cross-section. The aspect ratio of a nanowire is defined as $m = l/d$, where l is the length of the nanowire and d is its diameter. The demagnetization factors are given by[4]:

$$N_a = N_b = 4\pi \frac{m}{2\left(m^2-1\right)}\left[m - \frac{1}{2\left(m^2-1\right)^{1/2}} \ln\left(\frac{m+\left(m^2-1\right)^{1/2}}{m-\left(m^2-1\right)^{1/2}} \right) \right] \tag{1.8}$$

and:

$$N_c = 4\pi \frac{1}{2\left(m^2-1\right)}\left[\frac{m}{2\left(m^2-1\right)^{1/2}} \ln\left(\frac{m+\left(m^2-1\right)^{1/2}}{m-\left(m^2-1\right)^{1/2}} \right) - 1 \right] \tag{1.9}$$

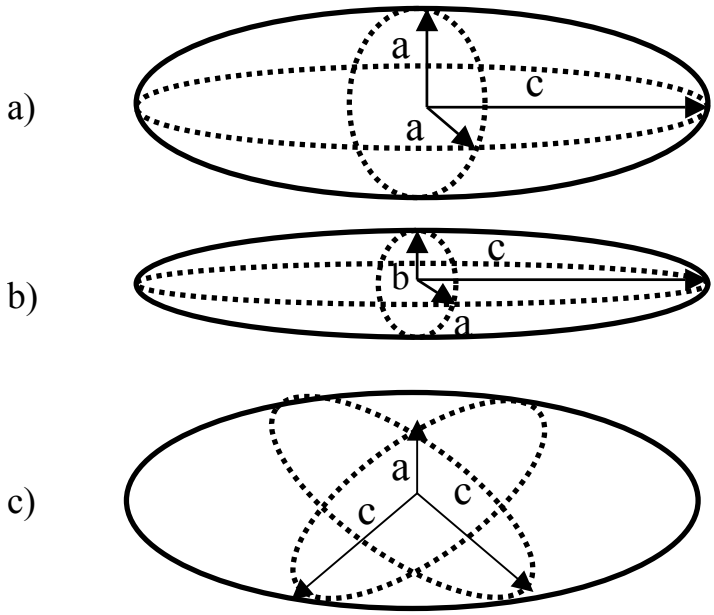

Figure 1.2 a) The prolate spheroid ($c > a = b$); b) The slender ellipsoid ($c >> a > b$); c) The oblate spheroid ($c = b > a$).

*b***.** *Slender ellipsoid*

This kind of ellipsoid (Figure 1.2.b) is a good approximation for nanowires that have a noncircular cross section. Its demagnetization factors are given by[4]:

$$N_a = 4\pi \frac{b}{a+b} - \frac{1}{2}\frac{ab}{c^2} \ln\left(\frac{4c}{a+b} \right) + \frac{ab\left(3a+b\right)}{4c^2\left(a+b\right)}, \tag{1.10}$$

$$N_c = 4\pi \frac{a}{a+b} - \frac{1}{2}\frac{ab}{c^2} \ln\left(\frac{4c}{a+b} \right) + \frac{ab\left(a+3b\right)}{4c^2\left(a+b\right)}, \tag{1.11}$$

and:

$$N_c = 4\pi \frac{ab}{c^2}\left[\ln\left(\frac{4c}{a+b}\right) - 1\right]. \qquad (1.12)$$

c. Oblate spheroid

This ellipsoid (Figure 1.2 c). is a good approximation for disc-shaped magnetic segments in multiple segment nanowires. As for the prolate spheroid its aspect ratio is $m = c/a$, and the demagnetization factors are given by the following equations [4]:

$$N_a = 4\pi \frac{m^2}{m^2 - 1}\left[1 - \frac{1}{\left(m^2 - 1\right)^{1/2}} \arcsin\left(\frac{\left(m^2 - 1\right)^{1/2}}{m}\right)\right] \qquad (1.13)$$

and:

$$N_b = N_c = 4\pi \frac{1}{2\left(m^2 - 1\right)}\left[\frac{m^2}{\left(m^2 - 1\right)^{1/2}} \arcsin\left(\frac{\left(m^2 - 1\right)^{1/2}}{m}\right) - 1\right]. \qquad (1.14).$$

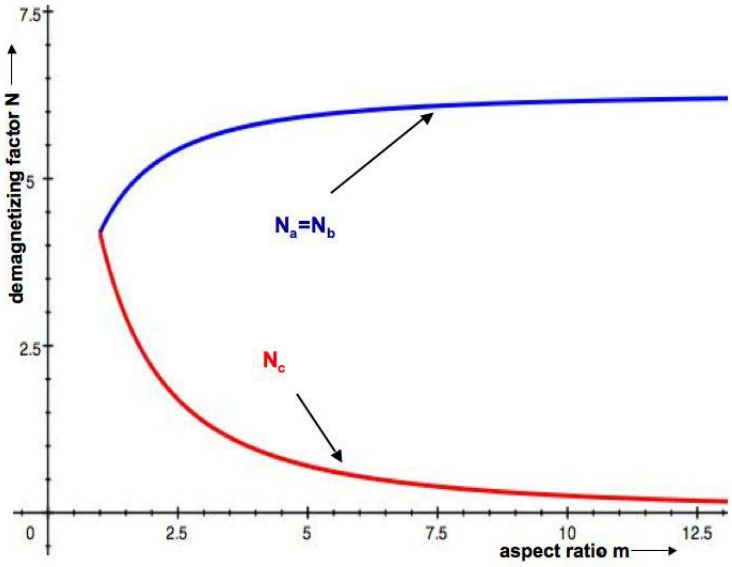

Figure 1.3 The demagnetizing factor (N) as function of aspect ratio (m) for a prolate spheroid.

In Figure 1.3 is represented the dependence of the demagnetizing factor with the aspect ratio for a prolate spheroid. A nanowire with a large value of the aspect ratio can be considered an infinitely long cylinder and can be assimilated to a prolate ellipsoid. The infinitely long cylinder approximation can be used for values of $m > 10$.

1.2.4 Zeeman Energy

Zeeman energy is the energy of the interaction between the magnetization vector and the external applied field, and is given by:

$$W_H = -\mathbf{M} \cdot \mathbf{H} \tag{1.15}$$

1.2.5 Exchange Energy

The notion of exchange interaction was first introduced by Heisenberg in 1928 to interpret the origin of the enormously large molecular fields acting in ferromagnetic materials.[2] This interaction is due to a quantum mechanical effect. The energy of exchange interaction is given by:

$$W_E = -2\sum_{ij} J_{ij}\mathbf{S_i}\mathbf{S_j}, \tag{1.16}$$

were $\mathbf{S_i}$ and $\mathbf{S_j}$ are spins. The term J_{ij}, which has no corresponding concept in classical physics, is called the exchange integral. Here $J_{ij} > 0$ brings two spins parallel to each other, phenomenon described as ferromagnetism, whereas $J_{ij} < 0$ brings two spins antiparallel to each other, phenomenon known as antiferromagnetism.

1.2.6 Magnetostatic Interactions among Nanowires.

In the previous paragraphs we analyzed the case of a single wire, assuming that the interaction between nanowires is negligible. The magnetic field $\mathbf{H}_x$ created by a dipole having a length l and a magnetic moment $\mathbf{m}$, at a certain distance x in the direction perpendicular to the dipole is given by equation 1.17 [4,13]:

$$\mathbf{H}_x = \frac{\mathbf{m}}{\left(x^2 + \frac{l^2}{4}\right)^{3/2}} \tag{1.17}$$

Here l is the length of the dipole, $\mathbf{m} = \mathbf{M}_s V$ is the magnetic moment and V is the volume of the dipole. This approximation gives a good estimation of the value of the magnetostatic interaction between two wires at a distance $\boldsymbol{x}$.

1.3 Magnetization Process

1.3.1 Stoner-Wohlfarth (SW) Model

With the basic concepts mentioned so far we are now able to describe some specific models to study the magnetization process of magnetic systems. It is well known that a magnetic material in general consists of many domains, or it has a multi-domain structure. This means that it is divided into uniformly magnetized regions or domains separated by domain walls in order to minimize its free energy.[14] The magnetization behavior of an assembly of a single domain ferromagnetic particles has been one of the central issues in the study of magnetism. Many different approaches and models were taken. Among these models the Stoner-Wohlfarth model is one of the basics. Usually a particle is called a Stoner-Wohlfarth or Stoner particle if the magnetic moments of all atoms are aligned in the same direction, creating a so-called single magnetic domain. In this mode the magnetization rotates in the same angle everywhere through the particle, and it is therefore known as the coherent rotation mode. This model can describe pretty well the system of small magnetic particles, when the thermal fluctuations of magnetic particles and the interactions between them are negligible. However, when one has to deal with the system of single domain particles with their sizes lower than some critical value, the thermal effect needs to be taken into account since in this case the thermal energy of the system would be comparable to the magnetic anisotropy energy barrier of single domain particles. The anisotropy

energy of a uni-axial single domain particle is given by: $E = KV \sin^2 \theta$, where K is the anisotropy constant, and θ is the angle between the magnetization vector and the easy axis. So, the energy barrier, separating easy directions is: $E_B = KV$ and is proportional to the volume V. Therefore, by decreasing the particle size, the anisotropy energy decreases, and for a domain size lower than a certain value, it may become comparable to or even lower than the thermal energy kT. This implies that the energy barrier for magnetization reversal may be overcome, and then, the magnetic moment of the particle can thermally fluctuate from one easy direction to another, even in the absence of the applied field, like a single spin in paramagnetic material. This type of behavior is called superparamagnetism.[14]

In 1948, starting with the assumption that is possible to identify all magnetic particles which reverse their magnetization by coherent rotation, Stoner and Wohlfarth came up with a model to describe such a system.[15] The basic idea of the Stoner-Wohlfarth model, is that a single magnetization vector is sufficient to describe the state of the whole system. This reduces the number of degrees of freedom to only one. This approach is somewhat idealized and should not be expected to give accurate prediction of the behavior of real systems. One can apply this model for a mono-domain particle in which the exchange interaction will be able to keep the elementary spins parallel to respect each other, so that the whole system can be considered uniform and having a big single magnetization vector. One notable exception of this model is that the temperature of the whole system is not taken into account or can be considered zero. This should be reasonable when the sizes of all particles are still large enough so that the thermal energy is negligibly small, compared to the anisotropy energy, $E = KV$. In this case the magnetic relaxation (or the superparamagnetism) can be disregard. Also the Stoner-Wohlfarth model does not take into account the interaction between particles.

1.3.2 Landau-Lifshitz-Gilbert (LLG) Equation

The behavior of the magnetization of a single domain ferromagnetic particle has been the subject of several studies. The Stoner-Wohlfarth model describes the system of single domain particles, provided that the coherent rotation condition is satisfied, and magnetic relaxation is neglected. This model does not say anything about two aspects: how the system will approach equilibrium and how the magnetization will react to time varying applied field.

Landau and Lifshitz proposed in their 1935 paper[16] an equation of motion for magnetization in a homogeneously magnetized body. This equation is useful because describes both the equilibrium position, and the dynamics of the moment reaching that position. In 1955 Gilbert modified this equation to overcome the unphysical solution for large damping parameters.[17,18] The LLG equation is a nonlinear differential equation so its analytical solutions can be found only in special cases.

The magnetic moment of an electron is related to spin momentum by:

$$\mathbf{m} = \gamma \mathbf{S} \tag{1.18}$$

with γ the gyromagnetic ratio for an electron, given by:

$$\gamma = \frac{-ge}{2mc}. \tag{1.19}$$

Here, e is the electron charge, m is the electron mass, c is the speed of light and g is the Lande splitting factor. The equation (1.18) is valid in both classical and quantum mechanics. The torque exerted on a magnetic moment **m** by a magnetic field **H** is:

$$\mathbf{T} = \mathbf{m} \times \mathbf{H} \tag{1.20}$$

The equation (1.18) and the equation (1.20) give an equation of motion for the magnetic moment of an electron spin:

$$\frac{d\mathbf{m}}{dt} = \gamma \mathbf{m} \times \mathbf{H} \tag{1.21}$$

The gyromagnetic equation (1.21), simply describes an instantaneous precessional motion of the magnetization vector. The applicability of this equation is not limited to the torque exerted by an external field. Any torque on a magnetic moment **M** can be written in the form (1.21), if we define an effective magnetic field:

$$\mathbf{H} = -\frac{\partial W(\mathbf{m})}{\partial \mathbf{m}} \tag{1.22}$$

where $W(\mathbf{m})$ is the potential energy of the system with respect to the work done by rotating the moment against whatever forces are present. Theoretical and experimental studies of the ferromagnetic properties identified five different energy terms:

$$W_{tot} = W_H + W_D + W_E + W_K + W_\sigma \tag{1.23}$$

Where W_H is the external field energy, W_D is the demagnetization energy, W_E is the exchange energy, W_K is the anisotropy energy and W_σ is the magnetoelastic energy, accounting for the changes in the magnetization field energy introduced by strains in the crystal lattice. The corresponding effective fields are:

$$\mathbf{H}_{\text{tot}} = \mathbf{H}_{\text{H}} + \mathbf{H}_{\text{D}} + \mathbf{H}_{\text{E}} + \mathbf{H}_{\text{K}} + \mathbf{H}_\sigma \tag{1.24}$$

The first two terms are magnetic fields, the last three are effective fields that have quantum origins.[17,18]

The equation (1.21) represents uniform undamped precession of the vector **m** about the axis of the field **H**. The observable behavior of the magnetization of a single domain ferromagnetic particle is that of alignment of **m** with **H**. This alignment is due to the collision between precessing electrons which takes place within particle. Therefore, it appears that the field does

not directly cause alignment; rather it causes precession of **m** about the axis of the field, which along with collision will produce alignment.

Landau and Lifshitz introduced a second term in the equation (1.21), the tendency of which is to align **m** and **H**. In their 1935 paper[16], they proposed an equation for the dynamic behavior of **m**, which included a term proportional to:

$$(\mathbf{m}\times\mathbf{H})\times\mathbf{m} = \mathbf{H}\cdot(\mathbf{m}\cdot\mathbf{M}) - (\mathbf{H}\cdot\mathbf{m})\cdot\mathbf{m} \tag{1.25}$$

The original form of Landau-Lifshitz equation is:

$$\dot{\mathbf{m}} = -\gamma\left[\mathbf{H}\times\mathbf{m} + \lambda\left(\mathbf{H} - \frac{(\mathbf{m}\cdot\mathbf{H})\cdot\mathbf{m}}{M_S^2}\right)\right] \tag{1.26}$$

The factor λ is a constant, of the same dimensions as M_S that characterizes the dipole-dipole interaction between the elementary magnetic moments, and is limited by the condition that $\lambda << M_S$. The dynamics of magnetization described by Landau-Lifshitz equation can explain the ferromagnetic resonance (FMR) phenomenon that we used in our study to characterize the Ni nanowire arrays.

1.4 Ferromagnetic Resonance

Ferromagnetic resonance, also known as the resonant absorption of the external electromagnetic radiation, occurs in ferromagnetic materials and is a phenomenon of microwave spectroscopy[19].

The Bohr frequencies of the corresponding quanta absorbed or emitted in the Zeeman transitions are given by the formula:

$$h\nu_{ik} = \hbar\omega_{ik} = W_i - W_k = \Delta W_{ik} \tag{1.27}$$

Where $h = 2\pi\hbar$, is the Planck constant, and $\omega_{ik} = 2\pi\nu_{ik}$ the cyclic Bohr frequency. The value of the energy difference is defined as:

$$\Delta W_{ik} = g\mu_B \Delta m_{ik} H \tag{1.28}$$

where g is the Lande factor, or the spectroscopic splitting factor, Δm_{ik} is the difference of the magnetic quantum numbers of the states i and k of a given multiplet, and the Bohr magneton is $\mu_B = \frac{e\hbar}{2mc} \cong 10^{-20}$(emu), with m and e being the mass and respectively the charge of the electron, and $\boldsymbol{c}$ the speed of light. Therefore, the Bohr frequency range is:

$$\omega_{ik} = \frac{g\mu_B}{\hbar} \Delta m_{ik} H_0 \tag{1.29}$$

The values of Δm_{ik} are limited by the selection rules to ±1 for transitions occurring for quantum numbers $i \neq k$.

For an applied external field H_0, the connection between the resonant frequency and the external field is[19]:

$$\omega_{res} = \gamma H_0 \tag{1.30}$$

Where:

$$\frac{g\mu_B}{\hbar} = g\frac{e}{2mc} = \gamma \tag{1.31}$$

It can be seen from the last two equations 1.30 and1.31, that for a definite field frequency; we can get the value of the resonant magnetic field as:

$$H_{res} = \frac{\omega_0}{\gamma} \tag{1.32}$$

We can observe from the formula of the resonant magnetic field that this one does not depend on the Planck constant.

1.4.1 General Formula for the Resonance Frequency

The equation of motion for the magnetic moment of an electron spin (1.21) can be written if we assume that the spins responsible for the ferromagnetism precess at a frequency ω_0 not in

the external field H_0, but in some internal effective field $\mathbf{H_{eff}}$, equivalent in its action to the external field:

$$\dot{\mathbf{M}} = \gamma(\mathbf{M} \times \mathbf{H_{eff}}) \tag{1.33}$$

If the free energy is W, the resonance frequency of the oscillation is[19]:

$$\omega_{res} = \gamma H_{eff} = \frac{\gamma}{M \sin\theta}\left[\frac{\partial^2 W}{\partial\theta^2}\frac{\partial^2 W}{\partial\varphi^2} - \left(\frac{\partial^2 W}{\partial\theta\partial\varphi}\right)^2\right]^{1/2} \tag{1.34}$$

Where θ, φ, ρ are the orientations in spherical coordinates.

1.4.2 The Influence of the Shape in the Resonance Frequency

As we saw earlier the demagnetizing factors of the samples are influenced by their geometry. In such a way the resonant frequency is also influenced. We can write that for an applied external magnetic field $\mathbf{H_0}$, the energy is:

$$W = -(\mathbf{M_s} \cdot \mathbf{H_0}) + \frac{1}{2}\left(N_x M_{sx}^2 + N_y M_{sy}^2 + N_z M_{sz}^2\right) \tag{1.35}$$

In the previous paragraph 1.2.3, when we referred to the demagnetizing factors we used some different notations for them. So, to be consistent some specifications are needed:

$$N_a = N_x$$
$$N_b = N_y$$
$$N_c = N_z$$

In the equation (1.35) the term $\mathbf{M_s}$ represents the saturation magnetization. As we established in the paragraph 1.2.3, the sum of the demagnetizing factors on the three axis is: $N_a + N_b + N_c = N_x + N_y + N_z = 4\pi$. By selecting the x-axis of the Cartesian system of coordinates as the polar axis, and assuming the magnetizing field $\mathbf{H_0}$ to be applied parallel to the z axis we have:

$$W = -M_s H_0 \sin\theta\sin\varphi + 0.5M_s^2(N_y \sin^2\theta\cos^2\varphi + N_z \sin^2\theta\sin^2\varphi + N_x \cos^2\theta) \quad (1.36)$$

where θ, φ are the polar and azimuthal angles, respectively which define the orientation of the magnetization vector.

The resonance frequency can be written then as[19]:

$$\omega_{res} = \gamma\left[\frac{N_y - N_x}{N_z - N_x}\left[M_s^2\left(N_z - N_x\right)^2 - H_0^2\right]\right]^{\frac{1}{2}} \cong \gamma M_s\left[\left(N_y - N_x\right)\left(N_z - N_x\right)\right]^{1/2} \quad (1.37)$$

In the case of a prolate ellipsoid the equation (1.37) takes the form:

$$\omega_{res} = \gamma\left[H_0 - M_s\Delta N\right] \quad (1.38)$$

with $\Delta N = N_z - N_x$.

1.4.3 The Influence of the Crystal Magnetic Anisotropy on the Resonance Frequency

From equation 1.1 we have: $W_K = K_0 + K_1 \sin^2\theta + K_2 \sin^4\theta + ...$

Taking as an example the case of an uni-axial single crystal with K_1>0, and having the magnitude of the field limited by the condition: $\left(N_y - N_x\right)M_s < H_0 < \frac{2K_1}{M_s} + \left(N_y - N_z\right)M_s$, then we get:

$$\left[\frac{\omega_{res}}{\gamma}\right]^2 = \left\{\left[\frac{2K_1}{M_s} + \left(N_y - N_z\right)M_s\right]^2 - H_0^2\right\}\frac{2K_1 + (N_x - N_z)M_s^2}{2K_1 + (N_x - N_z)M_s^2} \quad (1.39)$$

If: $H_0 \geq (2K_1/M_s) + (N_y - N_z)M_s$ then:

$$\left(\frac{\omega_{res}}{\gamma}\right)^2 = H_0^2 - \frac{2K_1H_0}{M_s} - \left(N_y - N_x\right)\left(H_0M_s - 2K_1\right) - M_s\left(N_y - N_z\right)\left[H_0 - \left(N_y - N_x\right)M_s\right] \quad (1.40)$$

For a prolate ellipsoid if: $H_0 \leq 2K_1/M_s - \left(4\pi - 3N_x\right)M_s$, then:

$$\left(\frac{\omega_{res}}{\gamma}\right)^2 = \left[2K_1/M_s - \left(4\pi - 3N_x\right)M_s\right]^2 - H_0^2 \quad (1.41)$$

And if, $H_0 \geq 2K_1 / M_s - M_s(4\pi - 3N_x)$, then:

$$\left(\frac{\omega_{res}}{\gamma}\right)^2 = H_0\left[H_0 - 2K_1 / M_s + (4\pi - 3N_x)M_s\right] \qquad (1.42)$$

1.4.4 The Influence of Domain Structure on the Resonance Frequency

In the previous paragraphs, in accordance with the conditions occurring in most experiments on ferromagnetic resonance, it was assumed that the external magnetizing field for the sample, as a whole, could be looked upon as a single ferromagnetic region of arbitrary magnetization.

In weak magnetizing fields there will be a multi-domain structure in the sample, corresponding to a smaller free energy than for the single domain structure. In this case, it is necessary to pay specific attention to the presence in the sample of transitional inter domain layers of finite thickness in which the direction of the vector of spontaneous magnetization changes continuously in accordance with a definite law. If an alternating magnetic field is applied perpendicular to the easy axis, the magnetizations running anti-parallel in the neighboring domains will precess in opposite direction about the axis of easy magnetization. If, at the same time, the alternating magnetic field is at right angles to boundaries, then the radio frequency components of the magnetization will be in phase only when they are at right angles to the boundaries, and in counter-phase when they are parallel to the boundaries.

1.4.5 Line Width of Resonance Absorption

The line width of resonance absorption is the distance ΔH on the field scale at $\omega =$ const., or the distance $\Delta\omega$ at H_0 = const., between the sides of resonance absorption curve at mid-height. The Landau –Lifshitz equation (1.26), can be written in the form:

$$\dot{\mathbf{M}} = -\gamma(\mathbf{M}\times\mathbf{H}) - \alpha\frac{\gamma}{M}\left[\mathbf{M}\times(\mathbf{M}\times\mathbf{H})\right] \qquad (1.43)$$

Where $\alpha = \frac{\lambda}{\gamma} M$ is a dimensionless damping parameter. The frequency satisfies the equation:

$$\omega^2 - i\omega\Delta\omega - \omega_{res}^2 = 0 \tag{1.44}$$

Here ω_{res} has the form given by the relation (1.34) and:

$$\Delta\omega = \left[\frac{d\omega}{dH}\right]\Delta H = \frac{\alpha\gamma}{M}\left[\frac{\partial^2 W}{\partial\theta\partial\varphi} + \frac{\partial^2 W}{\partial\varphi^2}\frac{1}{\sin^2\theta}\right] \tag{1.45}$$

is the width of the resonant absorption line.

Chapter 2: Experiment

In this chapter are presented the samples preparation methods, the experiments performed to measure the major hysteresis loop (MHL) using a vibrating sample magnetometer and the ferromagnetic resonance experiments performed using a X-band spectrometer.

All the samples and templates used in this study were prepared in Prof. Wiley's laboratory from Department of Chemistry by Dr. Xiequn Zhang and Ms. Jin-Hee Lim. First of all, various membranes were prepared by anodization procedure described below. The obtained membranes were used as templates in which the magnetic nanowire arrays were grown by chemical electrodeposition.

2.1 Anodized Alumina Oxide (AAO) Template Preparation

AAO templates were synthesized in two steps anodization procedure, as is presented in Figure 2.1.

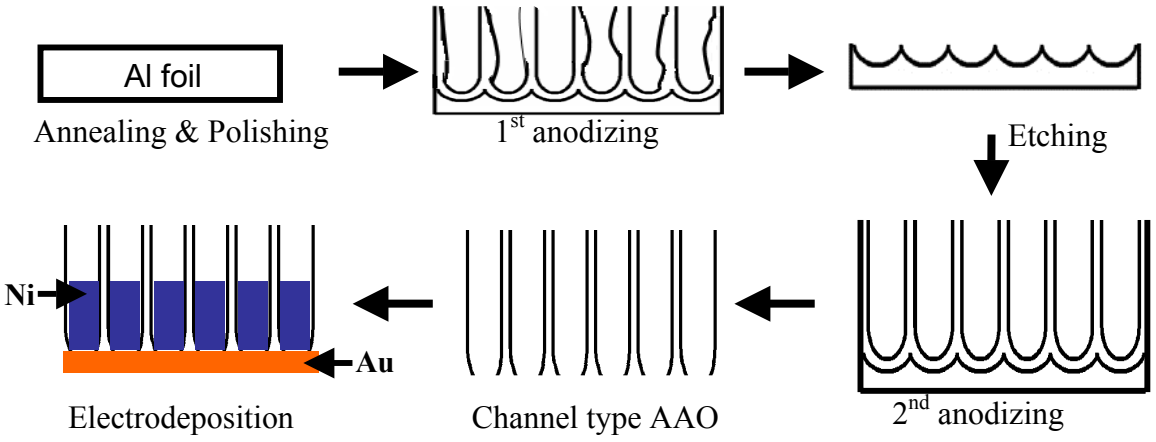

Figure 2.1 AAO templates preparation in two steps anodization.

A high purity aluminum foil (99.999%, Aldrich) was degreased in acetone for 20 min., then, it was annealed at 450° C under argon atmosphere for 5 h. The annealed Al sheet was

electropolished in a 1:4 mixture of $HClO_4$ and ethanol, at 25 V, and 10° C. After that, the sample was washed three times with distilled water and acetone. A mirror finished Al sheet was anodized at 40 V DC in 0.3 M $H_2C_2O_4$ at 17° C for 12 h. The oxide layer was removed by wet chemical etching process in a mixture of 5 wt% H_3PO_4 and 1.8 wt% CrO_3 at 70° C for 10 h. The Al remaining periodic concave patterns were anodized by using the same process, starting with the first step, to enable obtaining hexagonally ordered nanopore arrays of template (see Figure2.2).

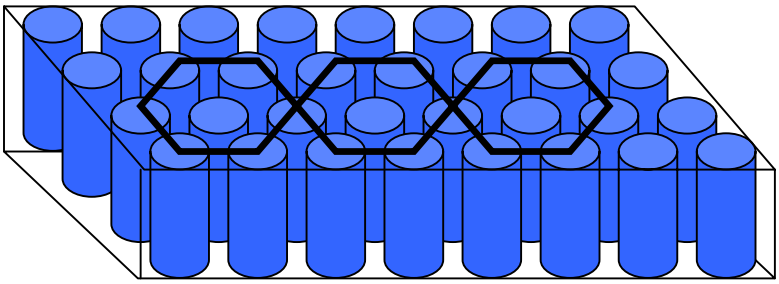

Figure 2.2 The hexagonally ordered nanopore arrays of the AAO template.

The Al film and barrier layer were separated into 1:1 mixture of $HClO_4$ and ethanol at 45 V and 10° C. The separated alumina template was washed three times with distilled water and acetone[20,21]. In order to obtain templates with the same interpore distance of 100 nm and different pore sizes, the templates were etched in 5 wt% H_3PO_4 solution at room temperature. The 40 nm sample was etched for 10 min., the 60 nm sample was etched for 30 min., and the 80 nm sample was etched for 50 min[22,23]. Then, the samples were washed thoroughly with large amounts of distilled water and acetone. The membranes produced following the above procedure are of much better quality than those commercially available, this is the reason we used them in

our studies. The hexagonally ordered pores can be observed in the Scanning Electron Microscope (SEM) images displayed in Figure 2.3.

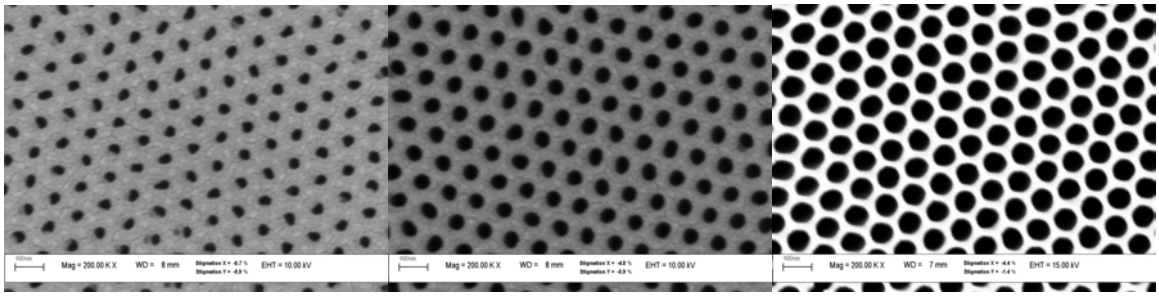

d=40 nm d=60 nm d=80 nm

Figure 2.3 The top surfaces of AAO templates with pore diameters of 40, 60, 80 nm, respectively, and interpore distance of 100 nm

2.2 Nanowire Electrodeposition

The Ni nanowires were electrodeposited into obtained AAO membranes, using an electrolyte composed of 120 g/l $NiSO_4$, 40 g/l H_3BO_4. Electrodeposition was performed in a three-electrode cell with Ag/AgCl reference electrode and a platinum wire counter electrode. The nanowires length was controlled by the charge during deposition [2,24]. The obtained samples consist of almost cylindrical and parallel sets of ferromagnetic Ni nanowires embedded in the alumina membrane (Fig. 2.4).

Two sets of Ni nanowires were prepared: one with the length of wires of 500 nm, and the other one with the length of 1000 nm. Each set was comprised by three kinds of samples with diameters of 40 nm, 60 nm and 80 nm, respectively. The interpore distance for each sample was 100 nm.

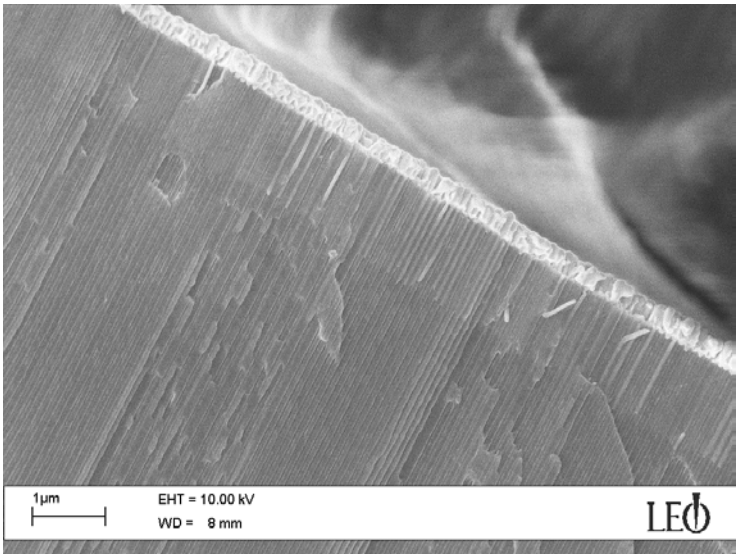

Figure 2.4 SEM image of Ni nanowire arrays of 60 nm diameter and 100 nm interpore distance.

2.3 Vibrating Sample Magnetometer (VSM) Measurements

The vibrating sample magnetometer (VSM) operates on Faraday's Law of Induction and is used to measure the magnetic behavior of materials. The changing magnetic field will produce an electric field that can be measured, and can provide information about the changing magnetic field. The static magnetic behavior of the nanowire samples was studied using the Vibrating Sample Magnetometer presented in Figure 2.5. The magnetic field was oriented at: 0^0 and 90^0 degrees with respect to the wire's axis. At 0^0 orientation, the field was parallel to the wires axis and at 90^0 , the field was perpendicular to the wires axis.

The measurements were performed at room temperature and the magnetic field for this measurement was chosen to sweep between -6000 Oe and +6000 Oe, because we observed that the saturation field for Ni was at 5000 Oe. The intervals chosen for the magnetic field (Oe), for the VSM measurement are presented in Table 2.1.

After doing the magnetostatic measurements it was observed for the sets of samples with length of 500 nm and 1000 nm that some properties of the samples such as the coercivity or the

saturation field change as the aspect ratio changes. The results of these measurements will be discussed in the next chapter.

Figure 2.5 Vibrating Sample Magnetometer, Lakeshore 7300 Series.

Field	Increment	Points
6000	-500	4
4000	-187.5	8
2500	-100	15
1000	-50	40
-1000	-100	15
-2500	-100	15
-4000	-50	40
-6000	50	40
-4000	187.5	8
-2500	100	15
-1000	50	40
1000	100	15
2500	187.5	8
4000	500	4
6000		

Table2.1 Magnetic field intervals (Oe) chosen for VSM measurements.

2.4 Ferromagnetic Resonance (FMR) Measurements

The dynamic properties of the Ni nanowires samples were studied using the ferromagnetic resonance. For this study, we used a Ferromagnetic Resonance (FMR) and Electron Paramagnetic Resonance (EPR) Spectrometer System, Bruker EMX 102, presented in Figure 2.6(b). The FMR measurements were performed at room temperature using X-band (9.8 GHz) FMR spectrometer at several orientations between -10^0 and 200^0, with the bias magnetic field applied parallel to wire's long axis for 0^0 orientation, and perpendicular to the wire's long axis for 90^0 orientation. The field was swept between 0 kOe and 9 kOe.

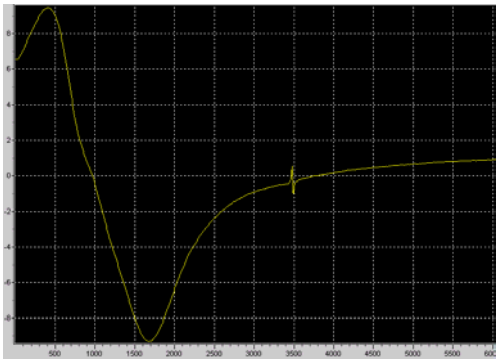

(a)

(b)

Figure 2.6(a) the FMR spectra for a sample of Ni nanowires with a diameter of wires of 120 nm, at 0^0 orientation and Figure 2.6(b) the FMR-EPR spectrometer system.

In order to observe the dependence of the resonance field on the angle of orientation of the applied field, we choose to perform the measurements at several angles. For both sets of samples it was observed that at 90^0 the resonant field has a minimum or a maximum value depending on the value of the aspect ratio. The results of these measurements will be discussed in the next chapter.

Chapter 3: Results and Discussions

This chapter presents the results of the major hysteresis loop measurements used to characterize the static properties of our samples. Then, the results of the ferromagnetic resonance measurements used to investigate the dynamic properties of the nanowire samples are presented. The measurements were performed in order to observe and analyze the interaction effects in magnetic nanowire.

3.1 Magnetic Measurements

Magnetic measurements were performed at room temperature using a VSM, for two series of Ni nanowires samples: one set with the length of wires of 500 nm, and the other set with length of 1000 nm.

3.1.1 Samples with the Length of Wires of 500 nm

The first set of samples analyzed had the length of wires of 500 nm. The first sample has wires with a diameter of 40 nm (sample d40l500), the second had a diameter of 60 nm (sample d60l500), and the third one had a diameter of 80 nm (sample d80l500). The magnetic field was applied parallel to the wire's long axis for the angle θ=0^0 and perpendicular to the wire's long axis for the angle θ=90^0.

a. Sample d40l500

The magnetization curve for the sample d40l500, presented in Figure 3.1, shows for a 0^0 orientation of the applied magnetic field, a coercive field, H_c = 0.558 kOe, and for 90^0 orientation the coercive field was H_c =0.148 kOe. The saturation field (H_{sat}) for the 0^0 orientation was 1.42 kOe, while for the 90^0 was 2.43 kOe. Because the value of H_c parallel is larger than the value of H_c perpendicular, and H_{sat} parallel value is smaller than H_{sat} perpendicular value, this sample

exhibits a preferential magnetic orientation along the wire's long axis[25]. The aspect ratio calculated in this case was $m = l/d = 12.5$.

For the parallel orientation, the measured remanent moment is $m_r = 0.448$ memu and the measured saturation moment for this orientation is $m_s = 0.531$ memu. The squareness ratio S is defined as:

$$S = \frac{m_r}{m_s} \tag{3.1}$$

For the sample d40l500 the calculated squareness ratio was $S = 0.84$.

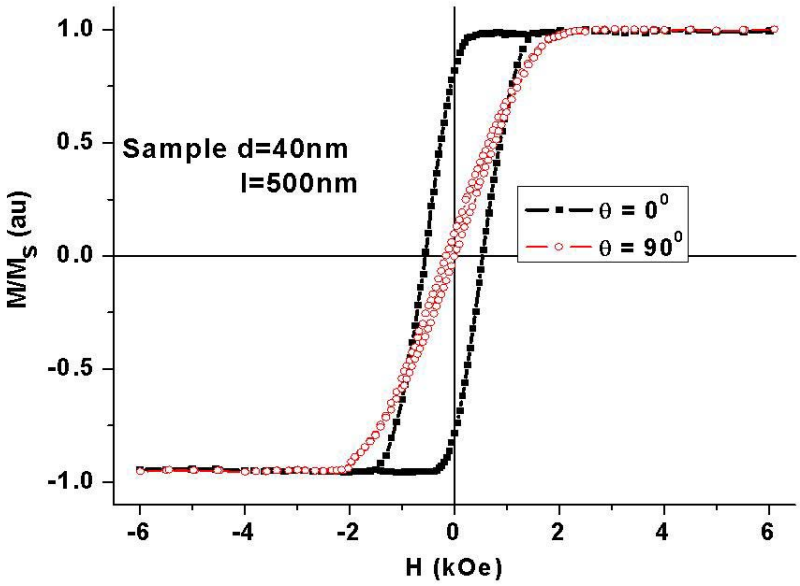

Figure 3.1 Hysteresis curve for the sample d40l500 measured at 0^0 and 90^0 orientation of the magnetic field.

b. Sample d60l500

The hysteresis curve for the sample d60l500, presented in Figure 3.2, exhibited at 90^0 orientation of the applied field a coercive field $H_c = 0.179$ kOe, and at 0^0, $H_c = 0.529$ kOe. The saturation field H_{sat} had a value of 1.4 kOe for the parallel orientation, and 1.9 kOe for the

perpendicular orientation. Therefore, this sample had a preferential magnetic orientation along the wire's principal axis. The saturation moment at 0^0 was m_s =0.647 memu, and the remanent moment at the same orientation was m_r = 0.514 memu. The calculated aspect ratio was m = 8.33 and the squareness ratio was S = 0.79.

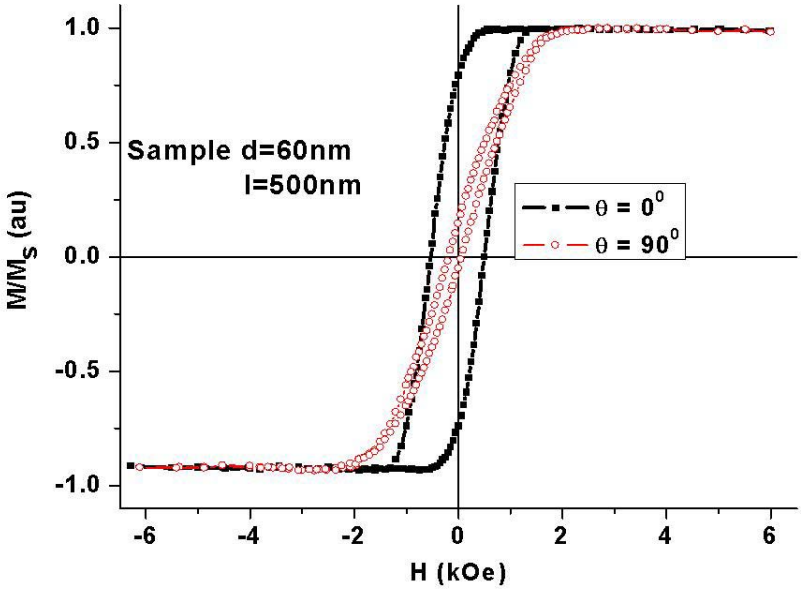

Figure 3.2 Hysteresis curve for the sample d60l500 at 0^0 and 90^0.

c. Sample d80l500

The magnetization curve for this sample (Figure 3.3) showed a coercive field for 90^0 H_c = 0.072 kOe, and for 0^0 H_c = 0.520 kOe. The saturation field had almost the same values for both directions of the applied field, H_{sat} = 2.1 kOe. The saturation moment at 0^0, in this case was m_s = 0.864, memu while the remanent moment for this sample, at the same orientation, was m_r = 0.365 memu. The calculated aspect ratio was m = 6.25 and the squareness ratio S = 0.43.

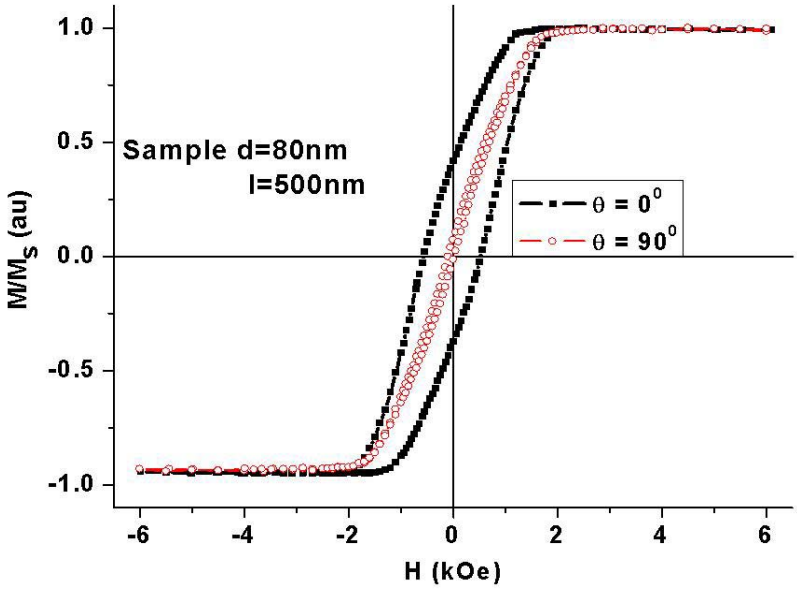

Figure 3.3 Hysteresis curve for the sample d80l500 at 0^0 and 90^0

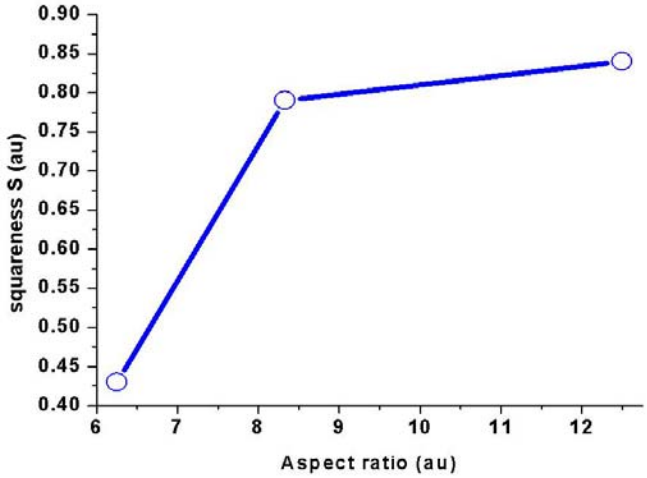

Figure 3.4 The squareness ratio *S* as a function of the aspect ratio *m* for the set of samples with the length of 500 nm.

Increasing the pore diameter from 40 nm to 80 nm, of this first set of samples while keeping the interpore distance constant we observed a decrease of the remanent moment m_r from

0.448 memu to 0.365 memu (almost 81%), as it was expected. In the same time the coercive field decreased for 0^0 orientation from 0.558 kOe to 0.520 kOe. The squareness ratio *S* increased as the aspect ratio *m* increased, namely as the pore diameter decreased (Figure 3.4).

3.1.2 Samples with the Length of Wires of 1000 nm

The second set of samples analyzed was composed of three samples of Ni nanowires with the same length of wires of 1000 nm and diameters of: 40 nm (sample d40l1000), 60 nm (sample d60l1000), and 80 nm (sample d80l1000), respectively. All three samples had the interpore distance of 100 nm. This set was measured using a VSM at room temperature with the applied field parallel to the wire's long axis for the angle $\theta=0^0$ and perpendicular to the wire's long axis for the angle $\theta=90^0$.

a. Sample d40l1000

The sample d40l1000 had the largest calculated aspect ratio m = 25. From the magnetization curve (Figure 3.5) the coercive field measured at 0^0 was H_c= 0.53 kOe, while at 90^0 it was H_c= 0.125 kOe. The saturation field at 0^0 was H_{sat}= 1.5 kOe, and at 90^0 it was H_{sat}= 4.5 kOe. This showed a preferential orientation along the principal axis of wires. The saturation magnetic moment at 0^0 was m_s= 1.55 memu and the remanent magnetic moment at the same orientation was m_r= 1.51 memu. The squareness ratio for the sample d40l1000 was S = 0.97.

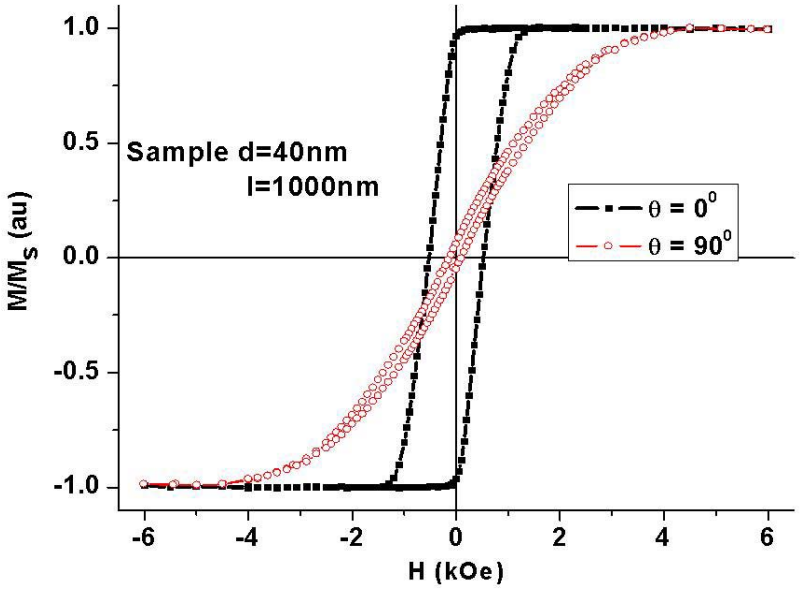

Figure 3.5 The hysteresis curve for the sample d40l1000 at 0^0 and 90^0

b. Sample d60l1000

For this sample the calculated aspect ratio was m = 16.7. The hysteresis loop of this sample (Figure 3.6), showed at 0^0 orientation a coercive field H_c = 0.616 kOe and at 90^0 H_c =0.075 kOe. The saturation field for the parallel orientation was H_{sat} = 2 kOe, and for perpendicular orientation H_{sat}= 3 kOe. This sample had also a preferential orientation along the principal wire's axis. At 0^0 the remanent magnetic moment was measured and found to be m_r = 1.3 memu and the saturation magnetic moment at the same orientation was m_s = 0.94 memu. The squareness ratio was S = 0.72.

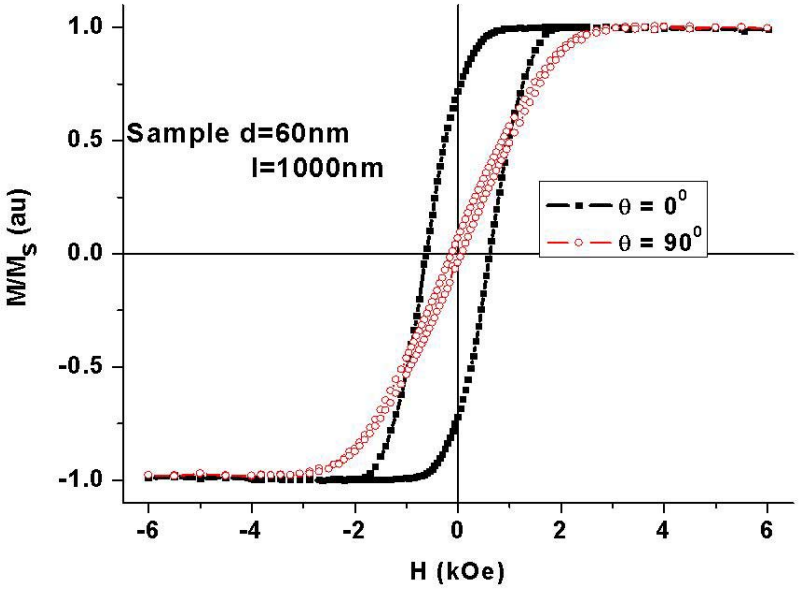

Figure 3.6 The hysteresis curve for the sample d60l1000 at 0^0 and 90^0

c. Sample d80l1000

For the sample d80l1000 the calculated aspect ratio was m = 12.5. From the magnetization curve of this sample (Figure 3.7) we observed that it had a coercive field H_c = 0.66 kOe at 0^0 and H_c = 0.083 kOe at 90^0 orientation of the applied field. The saturation field for both orientations exhibited almost the same value H_{sat} = 2.88 kOe. The saturation magnetic moment at 0^0 was m_s = 1.81 memu and the remanent magnetic moment for the same orientation of the applied field was m_r = 0.92 memu. In this case the squareness ratio had the value S = 0.5.

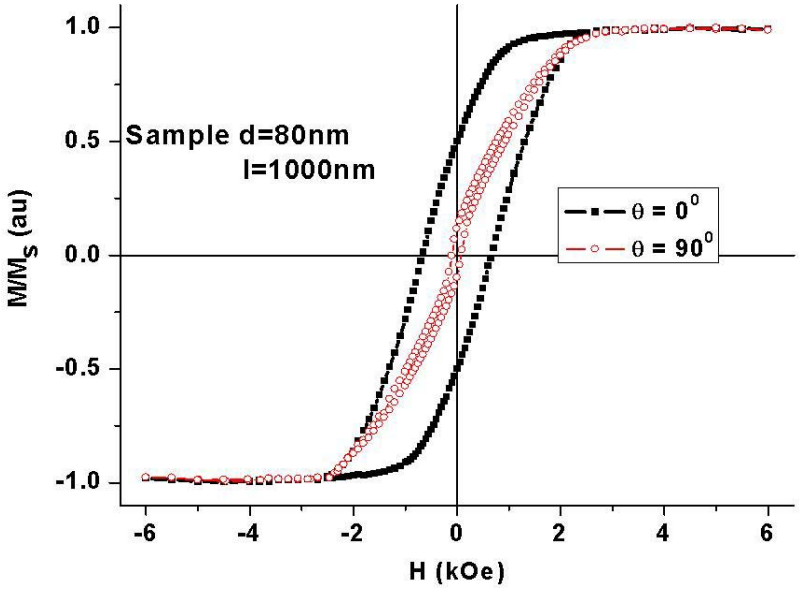

Figure 3.7 The hysteresis curve for the sample d80l1000 at 0^0 and 90^0

For the second set of samples, increasing the diameter from 40 nm to 80 nm, while keeping a constant interpore distance of 100 nm, induced a decrease of the remanent magnetic moment which was observed to range from 1.51 memu to 0.92 memu (almost 61%). In this case an increasing of the coercive field was noticed from 0.53 kOe to 0.66 kOe .

As expected, the squareness ratio *S* of this second set of samples increased as the aspect ratio *m* increased (Figure 3.8).

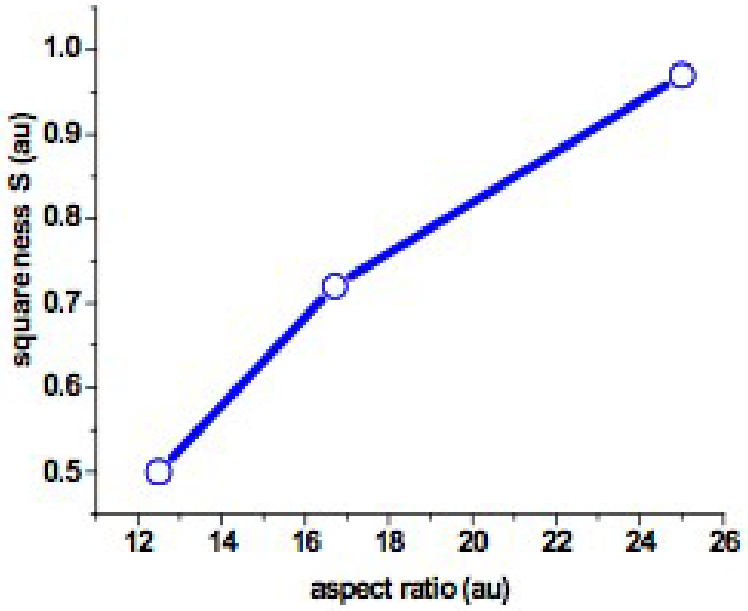

Figure 3.8 The squareness ratio vs apect ratio for the samples with length of 1000 nm

3.1.3 Conclusions of Magnetic Measurements

The two sets of samples exhibited different variations of the value of coercivity with the aspect ratio for the applied field parallel to the wires' long axis.

For the samples with the length of wires of 500 nm the coercivity decreased as the aspect ratio decreased. This can be explained taking into account that increasing the wires diameter while keeping the same interpore distance, the value of the demagnetization field increased, trying to change the preferential orientation perpendicular to the wire's long axis (Figure 3.9)

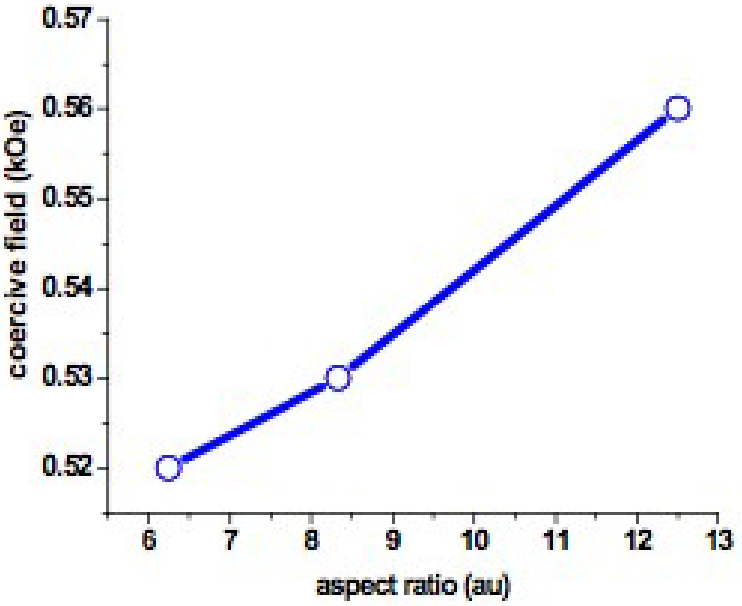

Figure 3.9 The coercive field as function of the aspect ratio for the set of samples with 500 nm length of wires.

For samples with the length of wires of 1000 nm the value of the coercivity increased as the aspect ratio decreased. For this set increasing the diameter of wires from 40 nm to 80 nm, while keeping the same interpore distance constant, the lateral surfaces of wires became more proximate and the interaction among them more important (Figure 3.10). For a system of long wires with the aspect ratio larger than 10, the interaction fields

among wires can significantly change the behavior of the whole system. The samples d40l500 and d80l100 have the same aspect ratio of 12.5, but their values of the coercivity for the field applied parallel are different. This value for the sample d80l100 is larger that the one of the sample d40l500. This can be explained that in the first case the interactions among wires are very

important and in the second case the demagnetization field inside the wires became very strong.

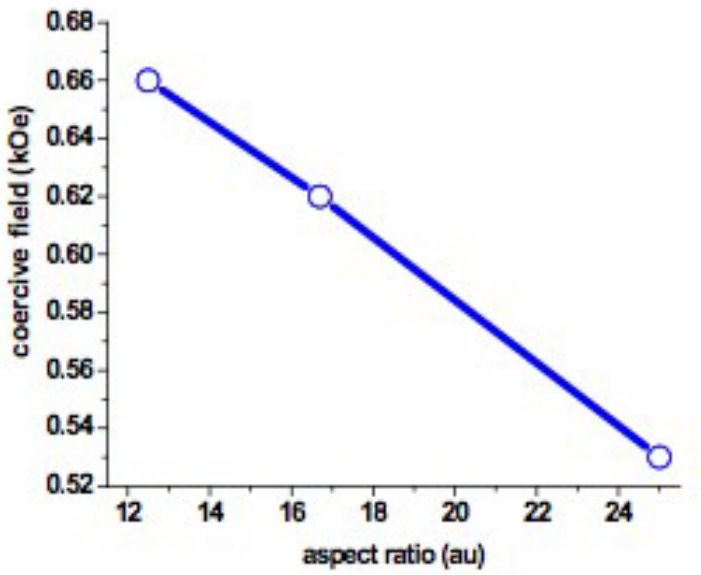

Figure 3.10 The coercive field as function of the aspect ratio for the set of samples with 1000 nm length of wires.

3.2 Ferromagnetic Resonance Measurements

The ferromagnetic resonance measurements, for both sets of samples were performed at room temperature using a X-band spectrometer, with the bias magnetic field applied along different directions with respect to wires' axis (parallel to the wires's long axis for the angle $\theta = 0^0$ and perpendicular to the wires's long axis for the angle $\theta = 90^0$).

3.2.1 Samples with the Length of Wires of 500 nm

a. Sample d40l500

The FMR spectra of this sample are presented in Figure 3.11. At 90^0 orientation, the value of the resonant field was 3.6 kOe, while for the 0^0 orientation the value of the resonant field was 2.2 kOe.

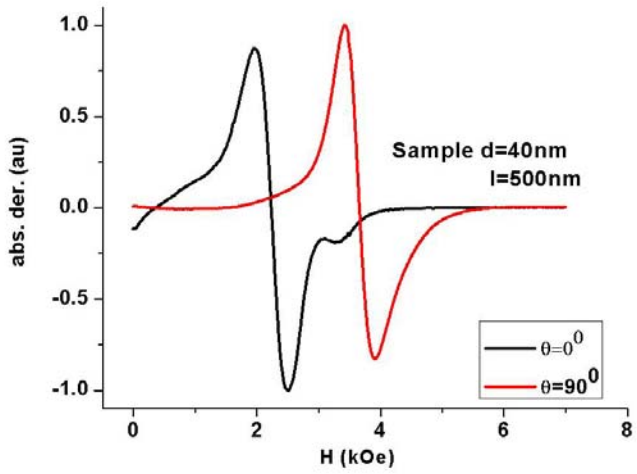

Figure 3.11 The FMR spectra of sample d40l500 for the parallel and perpendicular orientation of the bias applied field.

b. Sample d60l500

In the Figure 3.12 are presented the FMR spectra of the sample d60l500 for the both orientations. The value of the resonance field for the perpendicular orientation was 3.4 kOe and for the parallel one was 2.4 kOe.

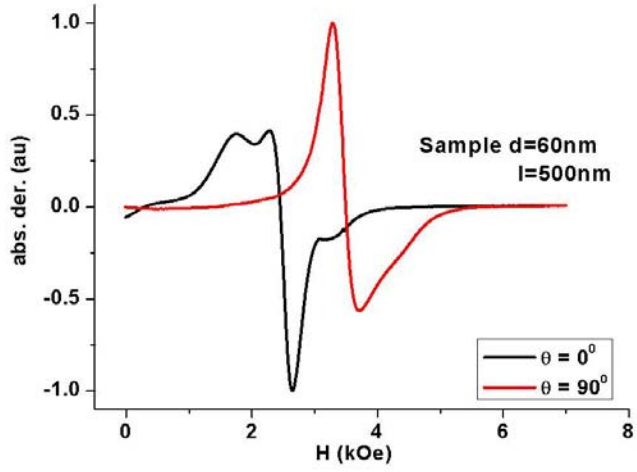

Figure 3.12 The FMR spectra of sample d60l500 for the parallel and perpendicular orientation of the bias applied field.

c. Sample d80l500

In the Figure 3.13 are presented the FMR spectra of the sample d80l500 for the both orientations. The value of the resonance field for the perpendicular orientation was 3.4 kOe and for the parallel one was 3.15 kOe.

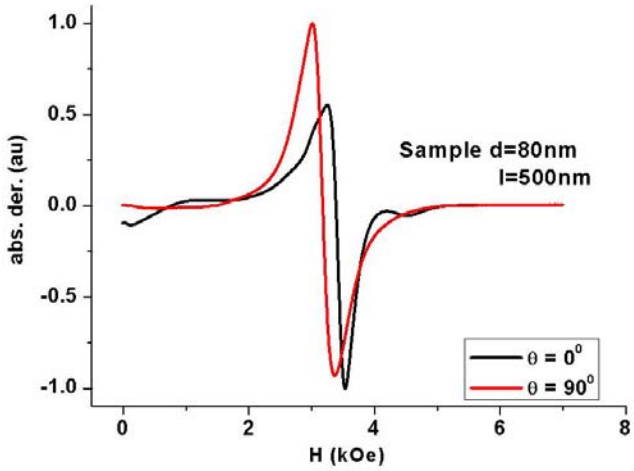

Figure 3.13 The FMR spectra of sample d80l500 for the parallel and perpendicular orientation of the bias applied field.

Unlike the previous two samples, the sample d80l500 exhibited a larger value of the resonance field for the parallel orientation than the one corresponding to the perpendicular one.

In Figure 3.14 are presented the angular dependence of the resonance field for the samples with the length of wires of 500 nm. It was observed that this angular dependence of the resonance field depends on the aspect ratio, flattening with the decrease of it.

A similar variation of the angular dependence of the resonance field was previously observed on two dimensional arrays of permalloy nano stripes prepared by electron beam nanolithography [26].

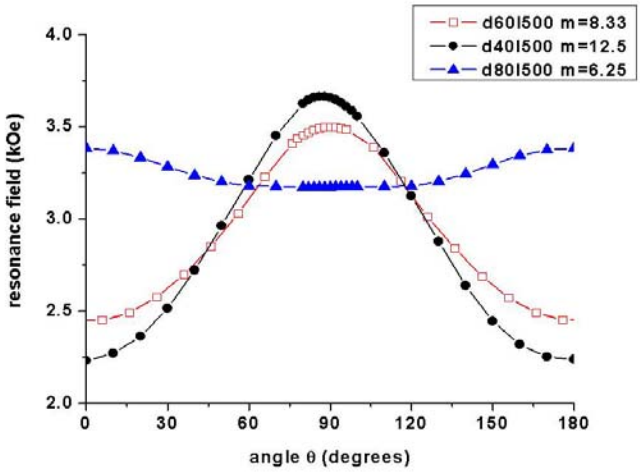

Figure 3.14 The angular dependence of the resonance field for the set of samples with the length of wires of 500 nm.

It was observed that not only the aspect ratio influences the value of the resonance field; we can see from the Figure 3.15 that the resonance field vs. aspect ratio is also a function of the orientation, decreasing with the increasing of the aspect ratio for the bias applied field parallel and increasing with the increasing of the aspect ratio for the perpendicular orientation of the bias applied field.

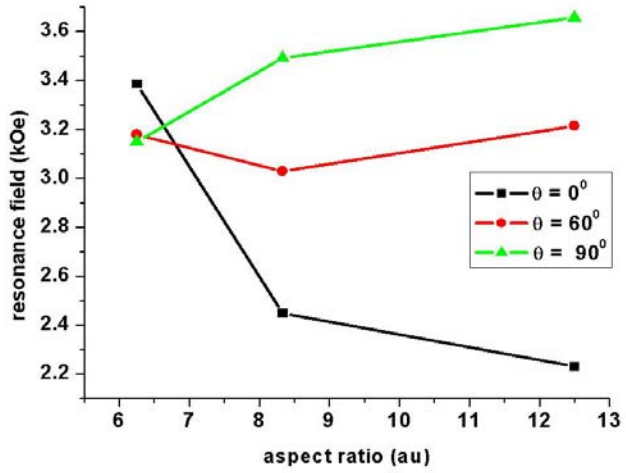

Figure 3.15 The angular dependence of the resonance field for the set of samples with the length of wires of 500 nm at different orientations.

3.2.2 Samples with the Length of Wires of 1000 nm

a. Sample d40l1000

FMR spectra of this sample (Figure 3.16), showed a value of the resonance field of 1.2 kOe for the parallel orientation and 4.4 kOe for the perpendicular orientation.

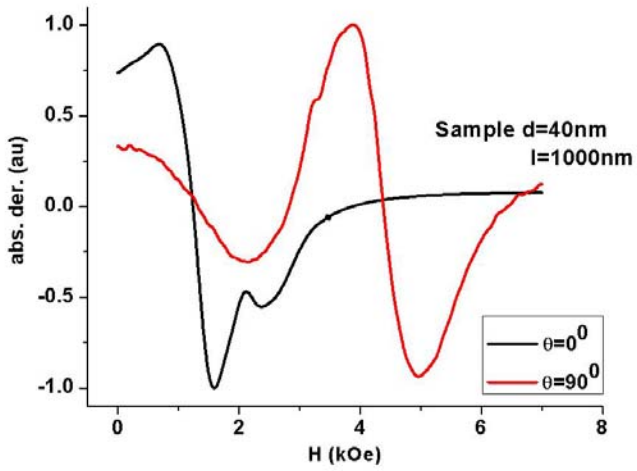

Figure 3.16 The FMR spectra of sample d40l1000 for the parallel and perpendicular orientations of the bias applied field.

b. Sample d60l1000

FMR spectra of this sample, presented in Figure 3.17, show a value of the resonance field of 2.45 kOe for the parallel orientation, and 3.6 kOe for the perpendicular orientation. As it was observed for the previous set of samples the value of the resonance field decreased in this case for the parallel orientation of the applied field and increased for the perpendicular configuration, but the difference between this two values became smaller than the one corresponding to the sample d40l100.

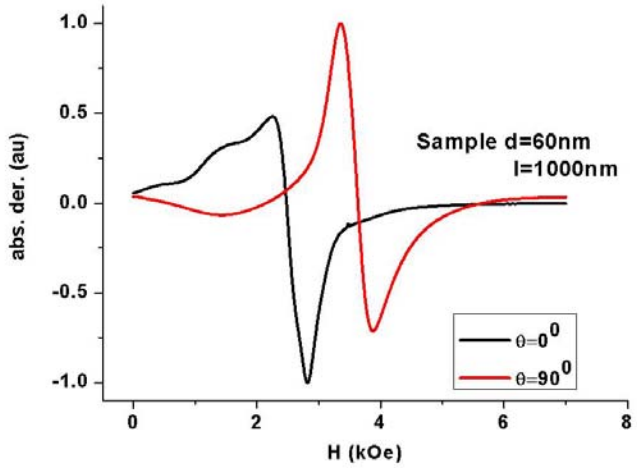

Figure 3.17 The FMR spectra of sample d60l1000 for the parallel and perpendicular orientations of the bias applied field.

c. Sample d80l1000

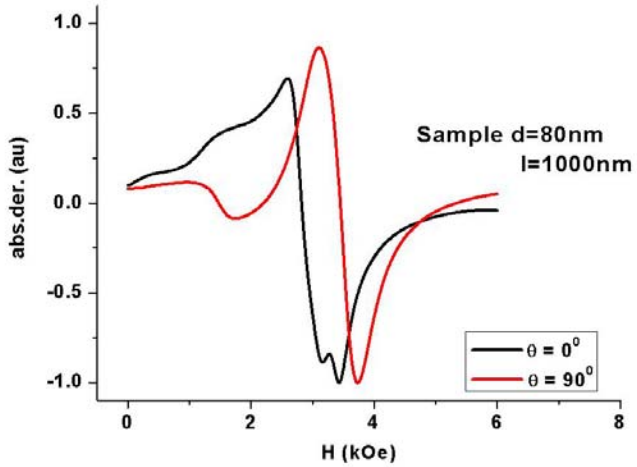

Figure 3.18 The FMR spectra of sample d80l1000 for the parallel and perpendicular orientations of the bias applied field.

FMR spectra of the sample d80l1000 (Figure 3.18), showed a value of the resonance field of 2.8 kOe for the parallel orientation and 3.4 kOe for the perpendicular orientation.

Like in the case of the set of samples with the length of wires of 500 nm, for the set of samples with 1000 nm length of wires the angular dependence of the resonance field was observed to flatten as the aspect ratio decreased, result showed in Figure 3.19.

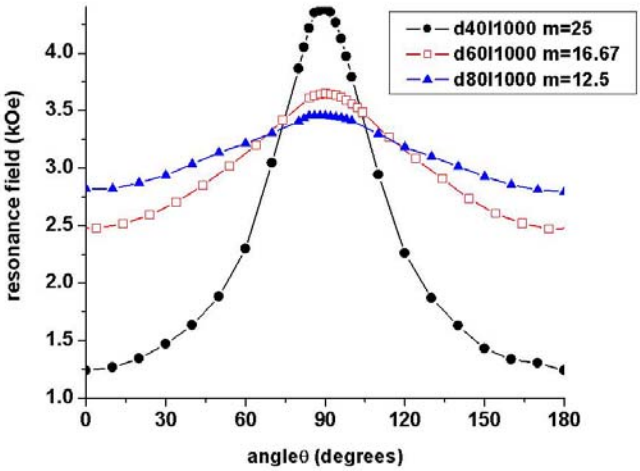

Figure 3.19 The angular dependence of the resonance field for the set of samples with the length of wires of 1000 nm.

Like for the first set of samples, the value of the resonance field was dependent also on the orientation of the applied field (Figure 3.20).

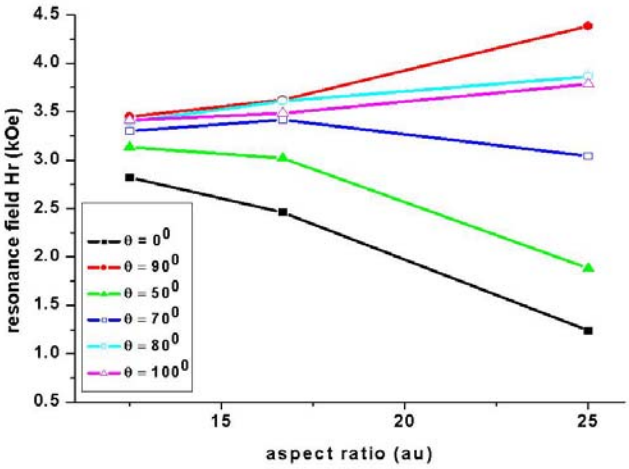

Figure 3.20 The angular dependence of the resonance field for the set of samples with the length of wires of 1000 nm at different orientations.

3.2.3 FMR Measurements Conclusions

For both sets of samples we observed a variation of the angular dependence of the resonance field, this one flattening as the aspect ratio decreased.

For the sample with the lowest aspect ratio (d80l500), the dipolar interactions were significant, they being able to cancel and even overcome the shape anisotropy, creating an easy axis perpendicular to the wires's long axis.

The orientation of the bias applied field influenced as well the value of the resonance field, this one decreasing as the aspect ratio increased for parallel orientation and increased with the aspect ratio for the perpendicular configuration for both sets of samples. This shows that the effect of interactions depends also on the orientation and that the interactions are more important when the field is applied along the principal axis of wires.

Chapter 4: Modeling of Interactions in Ferromagnetic Nanowire Arrays

This chapter discusses a theoretical model we proposed to explain our experimental results. As we observed, the properties of a nanowires system are strongly dependent on the geometry of the wires and also on the interactions between them. The interwire interactions are very complex, being very much dependent on the magnetization state of each wire.

A theoretical approach similar to that presented in Reference 8 was used to explain the angular dependence of the resonance field for both sets of samples. This work was done in collaboration with Dr. Ion Dumitru, former member of our group and currently an Assistant Professor at Iasi University, Romania. The main assumptions and parameters used in modeling the ferromagnetic resonance in these systems are given bellow.

4.1. Modeling of Interaction Effects

The nanowire assemblies were simulated using a 2D hexagonal lattice with approximately 7500 cylindrical wires (80x92) with an interwire distance D and the same diameter d and length l for all cylinders.

The saturation magnetization was taken as one for Ni, M_s = 485 emu/cm^3. The effective magnetic anisotropy of Ni nanowires was chosen to be uniaxial with $K_1 = 4.5 \times 10^5$ erg/cm^3 and easy axis parallel to the wire's long axis.[11] The magnetization is assumed to be uniform so that each wire of the assembly can be considered as a point dipole in the center of each cylinder.

The interaction field among wires and the demagnetization field were calculated in the center of each cylinder, using surface magnetic charge distributions that depend on the direction of the wire's magnetization.

The interaction field (assuming that all wires had the same direction of **M**) is given by:

$$\begin{bmatrix} H_{Ix} \\ H_{Iy} \\ H_{Iz} \end{bmatrix} = -\begin{bmatrix} N_{xx} & 0 & 0 \\ 0 & N_{yy} & 0 \\ 0 & 0 & N_{zz} \end{bmatrix}\begin{bmatrix} M_x \\ M_y \\ M_z \end{bmatrix} \tag{4.1}$$

where H_{Ix}, H_{Iy}, H_{Iz} are the interaction fields on *x, y* and *z* directions, N_{xx}, N_{yy}, N_{zz} are the demagnetization factors outside cylinders and M_x, M_y, M_z are the magnetizations on *x, y*, and *z* directions.[10]

The demagnetization field in the center of a wire is given by:

$$\begin{bmatrix} H_{Dx} \\ H_{Dy} \\ H_{Dz} \end{bmatrix} = -\begin{bmatrix} N_x & 0 & 0 \\ 0 & N_y & 0 \\ 0 & 0 & N_z \end{bmatrix}\begin{bmatrix} M_x \\ M_y \\ M_z \end{bmatrix} \tag{4.2}$$

where H_{Dx}, H_{Dy}, H_{Dz} are the demagnetization fields on *x, y* and *z* directions, N_x, N_y, N_z are the demagnetization factors inside cylinders and M_x, M_y, M_z are the magnetizations on *x, y*, and *z* directions. N_{zz} and N_z were calculated for each wire for a magnetization parallel to wire's long axis and N_{xx}, N_x were calculated for each wire for a perpendicular magnetization.[10] The demagnetization factors along x and y directions were considered equals ($N_{xx} = N_{yy}$ and $N_x = N_x$).

The total field inside each wire is the sum of the interaction field H_I, the demagnetization field H_D, the external applied field H_0, and the magnetocrystalline anisotropy field H_K.

The component of the imaginary part on *y* direction of the susceptibility tensor for each wire was determined using the formula[27]:

$$\chi = \frac{\omega}{\left(\omega^2 - \omega_{res}^2\right) + \omega^2\left(\Delta\omega\right)^2} \times \begin{bmatrix} -\gamma^2\left(1+\alpha^2\right)\Delta\omega\left(\dfrac{\partial^2 W}{\partial\varphi^2}\dfrac{\sin^2\varphi\cos^2\theta}{\sin^2\theta} - \dfrac{\partial^2 W}{\partial\varphi\partial\theta}\dfrac{\sin^2\varphi\cos\theta}{\sin\theta} + \dfrac{\partial^2 W}{\partial\theta^2}\cos^2\varphi\right) \\ +\alpha\gamma M_s\left(-\omega^2 + \omega_{res}^2\right)\left(\cos^2\varphi + \sin^2\varphi\cos^2\theta\right) \end{bmatrix} \tag{4.3}$$

We know from (1.45) that:

$$\Delta\omega = \left[\frac{d\omega}{dH}\right]\Delta H = \frac{\alpha\gamma}{M}\left[\frac{\partial^2 W}{\partial\theta\partial\varphi} + \frac{\partial^2 W}{\partial\varphi^2}\frac{1}{\sin^2\theta}\right]$$

and from (1.34) :

$$\omega_{res} = \gamma H_{eff} = \frac{\gamma}{M\sin\theta}\left[\frac{\partial^2 W}{\partial\theta^2}\frac{\partial^2 W}{\partial\varphi^2} - \left(\frac{\partial^2 W}{\partial\theta\partial\varphi}\right)^2\right]^{1/2}$$

In the formula (3.4) the terms $\frac{\partial^2 W}{\partial\theta^2}$, $\frac{\partial^2 W}{\partial\varphi^2}$ and $\frac{\partial^2 W}{\partial\theta\partial\varphi}$ are second derivatives of the free energy W .[19]

$$W = -\mu\mathbf{M}\cdot\mathbf{H}_{\mathbf{eff}} + \left|\frac{K_1}{\mathbf{M}\cdot\mathbf{H}_{\mathbf{eff}}}\right|\left(\mathbf{M}\cdot\mathbf{H}_{\mathbf{eff}}\right)^2 \qquad (4.4)$$

The total susceptibility is the sum of the susceptibilities of all wires. The external field was applied at different angles with respect to wire's axis and the dependence of the total susceptibility as function of the applied field at all orientations was plotted. The maximum of each curve determines the resonant field.

In Figure 4.1 are presented the simulated curves of the angular dependence of the resonance field for both sets of samples. We observe a very god agreement between the experimental and simulated data, the proposed model being able to describe very well the interactions in our magnetic nanowires with different strength of interactions.

As the interactions between nnaowires increase the angular dependence of the resonance field curve flattens, fact very well explained by the model.

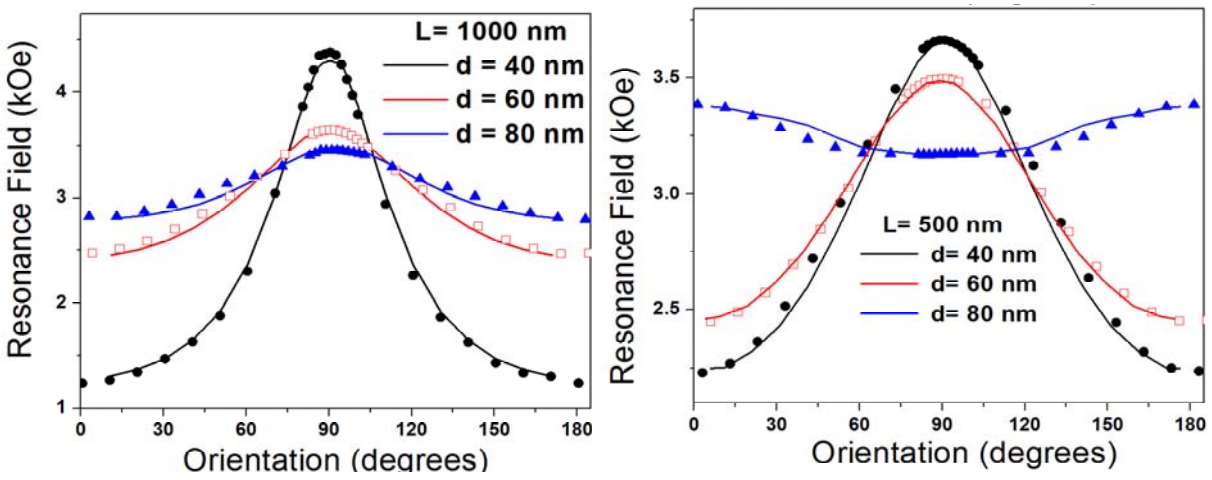

a. b.

Figure 4.1 Experimental (symbols) and simulated (lines) angular dependence of the resonance field for the samples with l=500 nm (a.) and l=1000 nm (b.)

Chapter 5: Conclusions and Future Work

Two different sets of Ni nanowire samples having the length of wires of 500 nm and 1000 nm, the same interpore distance of 100 nm, but different wire diameters of 40, 60 and 80 nm respectively, were investigated using ferromagnetic resonance and vibrating sample magnetometer.

The value of the coercivity for the applied field along the wires principal axes increased with the decreasing of the aspect ratio for the set of samples having the length of 1000 nm. This was explained taking into account the magnetostatic interaction among wires.

For the other set of samples (l = 500 nm), the value of the coercivity for the field applied parallel with wire axis decreased as the aspect ratio decreased and this was explained taking into account the increasing value of the demagnetization field.

The angular dependence of the ferromagnetic resonance field depends on the aspect ratio, flattening with the decrease of it.

It was observed that not only the aspect ratio influences the value of the resonance field, the orientation of the bias applied field influencing also these values.

Two different types of dependence of resonance field vs. aspect ratio were experimentally observed for different orientation of the applied field: the resonance field decreases with the aspect ratio when the field is applied parallel with wires' axis and increase when the field is perpendicular configuration. These show that the effect of the interactions depends on the orientation, the interactions being more important when the field is applied along wire's axis.

The simulated results showed the same angular dependence of the resonant field as we observed experimentally and were in good agreement with our experimental observation. We can conclude using our experimental and theoretical results that the value of the resonance field is strongly influenced by the aspect ratio value, interactions and also on the orientation of the applied field.

Future Work

Our next task is to investigate the behavior of more complex arrays composed of magnetic nanotubes and magnetic core-shell nanowires. In Figure 5.1 a) are presented empty magnetic nanotubes, and in Figure 5.1.b) are presented magnetic nanotubes filled with magnetic cores.

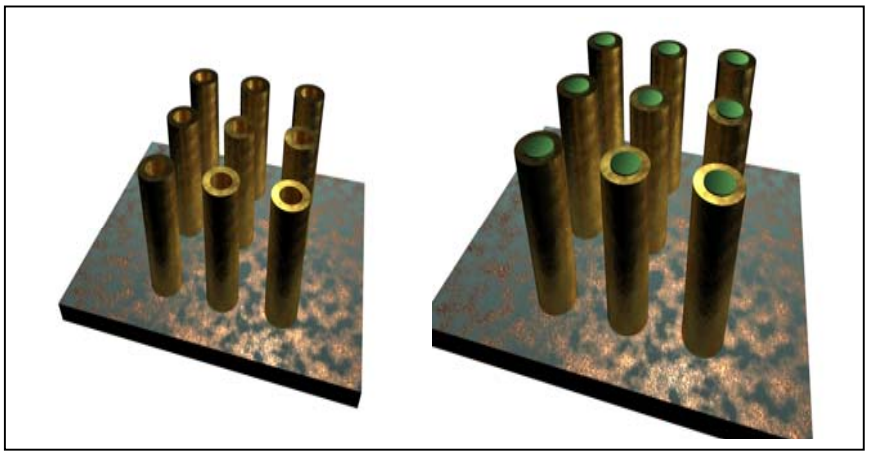

a b

Figure 5.1. Drawings of empty magnetic nanotubes (a) and magnetic nanotubes with magnetic core (b)

The preliminary measurements for a sample with Co shell and Ni core for the critical Curie temperature is presented in Figure 5.2. The temperature variation of magnetization confirms the existence of Co and Ni in our samples. However, for a complete characterization of such complex structures more detailed measured are needed. We plan to perform magnetic

measurements on single nanotube and single core-shell nanowires in collaboration with Dr. Wolfgang Wernsdorfer from Grenoble, France.

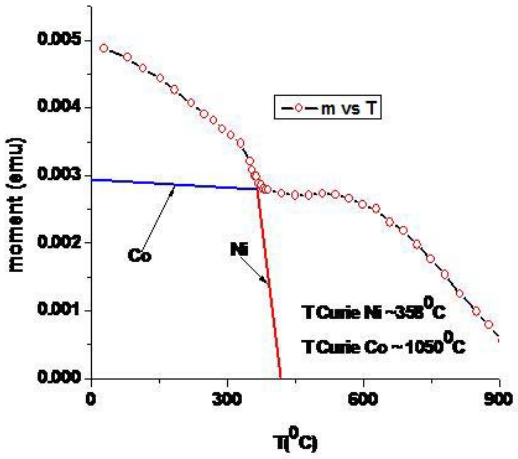

Figure 5.2 Magnetic moment vs. temperature for the sample Co nanotube with Ni core.

In Figure 5.2 the blue line represents the magnetic moment vs. temperature for cobalt only, and the red line represents the magnetic moment vs. temperature for nickel only.

References:

[1] D. Weller, A. Moser, L. Folks, M.E. Best, L. Wen, M. F. Toney, M. Schwickert, J-U. Thiele, M. F. Doerner, "High K_u materials approach to 100 Gbit/in^2", *IEEE Trans. Magn*., vol. 36, pp10-15, Jan 2000.

[2] A. Fert and L. Piraux, "Magnetic nanowires," *J. Magn. Magn. Mater.,* vol. 200, pp. 338-358, Oct 1999.

[3] R. O'Barr, S. Y. Yamamoto, S. Schultz, X. Weihua, A. Scherer, "Fabrication and characterization of nanoscale arrays of nickel columns", *J. Appl. Phys.,* vol. 81, pp. 4370-4376, Apr. 1997.

[4] L. Sun, Y. Hao, C. L. Chien, P. C. Searson, 'Tunning the properties of magnetic nanowires' IBM Journal of Research and development vol 49, pp 79-102 Ian 2005.

[5] G. C. Han, B. Y. Zong, and Y. H. Wu, "Magnetic properties of magnetic nanowire Arrays," *IEEE Trans. Magn.,* vol. 38, pp. 2562-2564, Sep 2002.

[6] G. Han, B. Y. Zong, P. Luo, and Y. Wu, "Angular dependence of the coercivity and remanence of ferromagnetic nanowire arrays," *J. Appl. Phys.,* vol. 93, pp. 9202-9207, Jun 1 2003.

[7] A. Encinas-Oropesa, M. Demand, L. Piraux, I. Huynen, and U. Ebels, "Dipolar interactions in arrays of nickel nanowires studied by ferromagnetic resonance," *Phys. Rev. B,* vol. 63, p. 104415, Mar 1 2001

[8] I. Dumitru, F. Li, J. B. Wiley, D. Cimpoesu, A. Stancu, and L. Spinu, "Study of magnetic interactions in metallic nanowire networks," *IEEE Trans. Magn.,* vol. 41, pp. 3361-3363, Oct 2005.

[9] I. Dumitru, L. Spinu, F. Li, J. B. Wiley, D. Cimpoesu, and A. Stancu, "Interaction effects analysis of FMR, spectra on dense nanowire systems," *IEEE Trans. Magn.,* vol. 42, pp. 3225-3227, Oct 2006.

[10] L. Carignan, C. Lacroix, A. Ouimet, M. Ciureanu, A. Yelon, and D. Menard, "Magnetic anisotropy in arrays of Ni, CoFeB, and Ni/Cu nanowires," *J. Appl. Phys.,* vol. 102, p. 10, Jul 2007.

[11] B. D. Cullity, *Introduction to magnetic materials,* 1st ed. (Adisson Wesley Pub. Comp, London, 1972, pp 103-432).

[12] Soshin Chikazumi and C.D. Graham, *Physics of Ferromagnetism*, 2nd ed. (Claredon Press: Oxford University Press, New York, 1997,ppxii, 655 p.)

[13] L. Cheng-Zhang, and L.C. Lodder, "The Influence of Packing Density on the Magnetic Behavior of Alumite Media," *J. Magn. Magn. Mater*., vol. 88, pp.236 , Nov 1990

[14] J.L. Dormann, D. Fiorani, and E. Tronc, Adv. Chem. Phys. (John Wiley and Sons Inc., New York,1977), Vol 98, pp.283-494.

[15] E.C.Stoner and E.P.Wohlfarth "A mechanism of magnetic hysteresis in heterogeneous alloys",Phil.Trans.Roy.Soc.A240,599-644 (1948)

[16] L.D.Landau and E.M.Lifshitz, "On the theory of the dispersion of magnetic permeability in ferromagnetic bodies" Phys.Z.Sowjet 8, 153-169 (1935)

[17] T.L.Gilbert, " A phenomenological theory of damping in ferromagnetic materials", IEEE Trans Magn. Vol 40, 3443-3449, (2004).

[18] T.L.Gilbert and J.M.Kelly, presented at the Conference on Magnetism and Magnetic Materials, Pittsburg, Pennsylvania, 1955 (unpublished)

[19] S. V. Vonsovskii, *Ferromagnetic Resonance*, 1st ed. (Pergamon Press Ltd. 1966, pp 4-131).

[20] L. Malkinski, A. Chalastras, A. Vovk, J.S. Jung, E.M. Kim, J.H. Jun, C.A. Ventrice Jr., " Magnetoresistive multilayers deposited on the AAO membranes", J. Magn. Magn. Mater. Vol 286, 108-112, Oct 2005.
[21] F. Li, L. Zhang and R. M. Metzger, "On the Growth of Highly Ordered Poresin Anodized Aluminum Oxide,"*Chem.Mater.,* vol.10, pp. 2470, Sep.1998.
[22] S. L. Oh, Y. R. Kim, L. Malkinski, A. Vovk, S. L. Whittenburg, E. M. Kim and J. S. Jung, *J. Magn. Magn. Mater*. Vol 310, 108-, (2007),
[23] H. Asoh, K. Nishio, M. Nakao, T. Tamamura and H. Masuda, " Growth of anodic porous alumina with square cells", *Journal of The Electrochemical Society*, vol. 48, pp. 3171-3174, Sep. 2004.
[24] J. I. Martin, J. Nogues, Lai Liu, J. L. Vicent, Ivan K. Schuller, " Orderes magnetic nanostructures: fabrication and properties", *J. Magn. Magn. Mater*, vol 256, pp 449-501, Aug, 2002.
[25] K. Nielsch, R. B. Wehrspohn, J. Barthel, J. Kirschner, U. Gosele, "Hexagonally ordered 100 nm period nickel nanowire arrays", *Appl. Phys. Lett*, vol 79, pp. 1360-1362, Aug 2001.
[26] L. M. Malkinski, M. H. Yu, A. Y. Vovk, D. J. Scherer, L. Spinu, W. L. Zhou, S. Whittenburg, Z. Davis, and J. S. Jung, "Microwave absorption of patterned arrays of nanosized magnetic stripes with different aspect ratios", *J. Appl. Phys*., vol. 101, p.09j110, May 2007.
[27] U. Netzelmann, "Ferromagnetic resonance of particulate magnetic recording tapes", *J. Appl. Phys.* vol 68, pp 1800-1807, Aug 1990.

Vita

The author was born in Cluj-Napoca, Romania, in 1963. He received his high school diploma in 1982 from G. Cosbuc High School in the same city and then enrolled at Technical University of Cluj-Napoca. He completed his bachelor in Metallurgical Engineering in 1989. After the graduation he worked as engineer for several Romanian and international companies. Between 1996 and 1999 he pursued a Master of Business and Administration at "Babes-Bolyai" University in Cluj-Napoca, Romania. To further enhance his education, he applied to University of New Orleans and became a graduate student starting in August 2004. In May 2008 he completed his Master of Science in Physics.